A mantle melting profile across the Basin and Range, SW USA

K. Wang,[1] T. Plank,[2,3] J. D. Walker,[1] and E. I. Smith[4]

Received 29 September 2000; revised 26 April 2001; accepted 27 June 2001; published 22 January 2002.

[1] The major and trace element composition of late Cenozoic basalts (0–10 Ma) across the Basin and Range province (B&R) preserve a clear signal of mantle melting depth variations. FeO, $Fe_{8.0}$, and Tb/Yb increase, whereas $Si_{8.0}$ and $Al_{8.0}$ decrease, from west to east across the B&R along a profile at 36°–37°N. These variations are qualitatively consistent with shallower melting beneath the Western Great Basin (WGB) than in the central B&R. In order to quantify the depth range and percent of decompression melting, we invert primary Na_2O and FeO contents of basalts using a melting model based on the partitioning of FeO and MgO in olivine and Na_2O in clinopyroxene. An independent inversion, using the rare earth elements (REE), corroborates the melting depths obtained from the major element model and places most of the melting beneath the central B&R in the garnet-peridotite stability field. We find that the shape of the melting region across the B&R closely mimics the shape of the mantle lithosphere, as inferred from geological and geophysical observations. Melting across the study area occurs largely within the asthenosphere and generally stops at the base of the mantle lithosphere. In the WGB, melting paths are shallow, from 75 to 50 km, and in some cases extend almost to the base of the crust. These melting paths are consistent with adiabatic melting in normal-temperature asthenosphere, beneath an extensively thinned (or absent) mantle lithosphere. Shallow melting is consistent with geobarometry and isotopic compositions of local mantle xenoliths. Lithospheric thinning was caused by thermal erosion during Mesozoic subduction and/or simple shear or foundering during Cenozoic extension. In contrast, melting beneath the central B&R occurs beneath thick mantle lithosphere and requires mantle potential temperatures 200°C hotter than normal (melting paths from 140 to 100 km). The excess temperature beneath the central B&R is consistent with active upwelling of hot mantle in this region. *INDEX TERMS:* 1025 Geochemistry: Composition of the mantle, 8120 Tectonophysics: Dynamics of lithosphere and mantle—general, 9350 Information Related to Geographic Region: North America, 3640 Mineralogy and Petrology: Igneous petrology; *KEYWORDS:* Mantle, melting, petrology, Basin and Range, lithosphere, extension

1. Introduction

[2] Although much progress has been made in developing mantle melting models for the generation of mid-ocean ridge basalts (MORB) [e.g., *Klein and Langmuir*, 1987; *McKenzie and Bickle*, 1988; *Langmuir et al.*, 1992; *Kinzler and Grove*, 1992; *Kinzler*, 1997; *Hirschmann et al.*, 1999], the conditions of melting that lead to magmatism during continental extension remain poorly understood. One of the most extensively studied regions of continental extension is the Basin and Range (B&R) province, where recent work has focused on structure of the upper mantle [*Humphreys and Dueker*, 1994a, 1994b; *Zandt et al.*, 1995; *Jones and Phinney*, 1998; *Wernicke*, 1992; *Jones et al.*, 1992; *Savage and Sheehan*, 2000; *Humphreys*, 1995; *Humphreys et al.*, 2000; *Lowry et al.*, 2000]. It is generally accepted that the lithosphere has been thinned during the past 15 Myr and that Cenozoic volcanism is related to extension [e.g., *Wernicke*, 1992; *Wernicke et al.*, 1988; *Gans and Bohrson*, 1998; *Best and Christiansen*, 1991; *Scott et al.*, 1995; *Jones*, 1987; *Hawkesworth et al.*, 1995; *Zandt et al.*, 1995; *Walker and Coleman*, 1991; *Walker et al.*, 1995]. Despite the general association between extension and volcanism, it has been difficult to constrain the depth and extent of mantle melting that leads to B&R basaltic magmatism. Part of the reason for this is that many other factors contribute to the genesis and evolution of continental basalts. For example, crustal contributions may partially or completely mask the composition of magma formed in the mantle [e.g., *Farmer et al.*, 1989, 1995; *Glazner et al.*, 1991; *Glazner and Farmer*, 1992], and even without crustal contamination, there is debate concerning the role of mantle plumes [e.g., *Bradshaw et al.*, 1993; *Feuerbach et al.*, 1993; *Parsons et al.*, 1994] and lithospheric versus asthenosphere mantle in B&R basalt genesis [e.g., *Hawkesworth et al.*, 1990; *Dungan et al.*, 1986; *Fitton et al.*, 1991; *Kempton et al.*, 1991; *Ormerod et al.*, 1991; *DePaolo and Daley*, 2000].

[3] This paper focuses on the depth of mantle melting as a means to discriminate between the various models for melting beneath the B&R. The depth of melting is a critical parameter, as it may reveal both mantle temperature and the lithosphere-asthenosphere boundary. During adiabatic decompression the base of the melting regime corresponds to the mantle solidus, which is largely a function of the potential temperature of the mantle [*McKenzie and Bickle*, 1988], whereas the top of the melting regime may correspond to the base of the rigid lithosphere, which impedes upwelling. Previous results on the depth of melting beneath the B&R are based on the distribution of alkali basalts versus tholeiites [e.g., *Perry et al.*, 1987; *Daley and DePaolo*, 1992; *Feuerbach et al.*, 1993; *DePaolo and Daley*, 2000] and approx-

[1]Department of Geology, University of Kansas, Lawrence, Kansas, USA.
[2]Formerly at Department of Geology, University of Kansas, Lawrence, Kansas, USA.
[3]Department of Earth Sciences, Boston University, Boston, Massachusetts, USA.
[4]Department of Geosciences, University of Nevada, Las Vegas, Nevada, USA.

0148-0227/02/2001JB000209$09.00

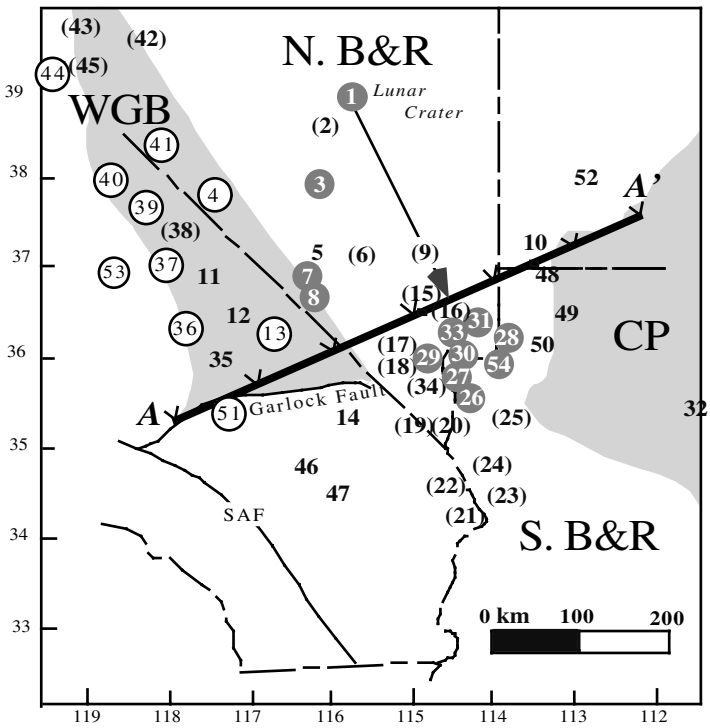

1: Lunar Crater
2: Pancake Range
3: Reveille Range
4: Clayton Valley
5: Nellis Air Force Range
6: Nye Canyon
7: Crater Flat
8: Lathrops Wells
9: Delamar Range
10: Hurricane
11: Saline Range
12: Pinto Peak
13: Death Valley
14: Cima
15: Las Vegas Range
16: Black Point
17: Las Vegas
18:McCulloough Range
19: Castle Mtns
20: Newberry Mtns
21: Parker
22: Needles Mtn
23: Lake Havasu
24: Black Mtn
25: Kingman
26: Mtn Perkins
27: Black Mtn
28: Grand Wash Trough
29: Fortification Hill
30: Wilson Ridge
31: Gold Butte
32: Sunset Crater (SC)
33: Hamblin-Callville Mesa
34: Eldorado Mtn.
35: Coso Range
36: Owens Lake
37: Big Pine
38: Bishop
39: Long Valley
40: Mono Lake
41: Mina
42: Fallon
43: Reno
44: Lake Tahoe
45: Carson City
46: Pisgah
47: Amboy
48: Washington Fault
49: Dellengbaugh fault
50: Toroweap fault
51: Lava Mountain
52: Markagunt
53: Kings River
54: Pakoon Springs

Figure 1. Location of late Cenozoic volcanic fields in the SW United States: WGB (shaded), Western Great Basin; B&R, Basin and Range; CP (shaded), Colorado Plateau; SAF, part of the San Andreas Fault. In following figures, locations are projected onto line A-A′ (as for Lunar Crater), with distances measured from A (ticks mark: 100 km). Solid circles denote volcanic fields with $Fe_{8.0}$ > 11 wt % (indicative of deep, hot melting). Open circles denote volcanic fields with $Fe_{8.0}$ < 9 wt % (indicative of shallow melting). Numbers with no circle are for volcanic fields with intermediate $Fe_{8.0}$. Numbers in parentheses are for volcanic fields with insufficient data. See Figure 3 for definition of $Fe_{8.0}$ and Table 1 for all values.

imate calibration to peridotite melting experiments (e.g., tholeiitic basalts are derived from mantle depths <60 km, whereas alkali basalts are derived from depths >60 km [*Takahashi and Kushiro*, 1983]). Other approaches rely on isotopic and trace element compositions of magmas as indicative of a melting within the lithosphere versus. asthenosphere [e.g., *Perry et al.*, 1987; *Farmer et al.*, 1989; *Rogers et al.*, 1995; *DePaolo and Daley*, 2000].

[4] Over the past 15 years, relatively precise parameters have been developed to quantify the conditions of melting beneath mid-ocean ridges [*Klein and Langmuir*, 1987; *McKenzie and Bickle*, 1988; *Langmuir et al.*, 1992; *Niu and Batiza*, 1991; *McKenzie and O'Nions*, 1991; *Asimow et al.*, 1995; *Hirschmann et al.*, 1998, 1999]. Recent experimental studies have also greatly improved our ability to quantify the conditions of melting up to 4 GPa [*Baker and Stolper*, 1994; *Hirose and Kushiro*, 1993; *Kinzler and Grove*, 1992; *Kinzler*, 1997; *Robinson et al.*, 1998; *Walter*, 1998; *Klemme and O'Neill*, 2000]. For example, melts from deep and hot mantle have higher FeO contents than those from relatively shallower mantle, and the experimentally determined phase equilibria permit calibration between FeO and *P* and *T* of melting [e.g., *Langmuir et al.*, 1992]. Therefore, Fe as well as other major and trace elements have been used to determine mantle melting depths for not just mid-ocean ridge basalts but also ocean island basalts [e.g., *Hauri*, 1996] and continental basalts [*Fram and Lesher*, 1997].

[5] *Rogers et al.* [1995] applied similar methodology to basalts from the Western Great Basin (WGB). They found a clear distinction between basalts from the WGB, which have low FeO, low TiO_2, and high SiO_2, and alkali basalts from the central and southern B&R. *Rogers et al.* [1995] developed a semiquantitative model for melting depth based on the silica content of basalts and the peridotite melting experiments of *Hirose and Kushiro* [1993], which show the dramatic effect of pressure on lowering SiO_2 melt concentrations. This comparison suggested segregation depths of 45–75 km for the Big Pine primitive basalts from the WGB and 90+ km for Geronimo alkali basalts from the B&R. Results are semiquantitative because fractionated basalts are not strictly comparable to primary and isobaric experimental melt compositions, and further complications will arise from variations in mantle source fertility or volatile content. Thus this use of silica as a melt generation barometer is at best indicative. Nonetheless, *Rogers et al.* [1995] combined these inferences from SiO_2 with other trace element and isotopic ratios to argue that melting occurs in the lithosphere beneath the WGB and in the deeper asthenosphere beneath the B&R.

[6] This paper aims to build on the earlier work of *Perry et al.* [1987] and *Rogers et al.* [1995] to develop a mantle melting profile across the B&R province. Such an effort is warranted owing not just to the recent experimental and modeling literature on mantle melting but also to a significant increase in the number of analyzed basalts from the southwest United States. For example, in the WGB alone, the number of analyzed basalts has doubled since the study of *Rogers et al.* [1995]. We have a particularly large data set ($n \approx 1000$) for basalts from 35° to 38°N in the B&R (Figure 1). The expanded data distribution makes it now possible to explore mantle melting quantitatively in a continuous ~550 km transect (Figure 1) across the B&R province. Our focus is on basaltic volcanism that has occurred over the last 10 Myr only.

2. Analysis and Data Compilation

[7] Approximately 400 samples from the western United States have been collected and analyzed by the Center for Volcanic and

Table 1. Compositional Parameters and Calculated Pressure/Depth of Melting for Basalt Groups Across the Basin and Range[a]

Basalt Group	Location	$Na_{8.0}$, wt %	Na_{prim}, wt %	$Fe_{8.0}$, wt %	Fe_{prim}, wt %	Mg_{prim}, wt %	$Si_{8.0}$, wt %	$Al_{8.0}$, wt %	Tb/Yb, CN	Epsilon, Nd	Distance, km	P_o, GPa	P_f, GPa	Z_o, km	Z_f, km	References[b]
Kings River	53	2.82	2.63	7.5	9.4	14.0	51.6	13.5			12	1.6	0.6	56	24	1
Tahoe(w)	44	3.40	3.41	8.3	8.5	8.5	50.6	16.3	1.58	0.4	30	2.3	1.5	75	52	2, 3, 4
Mono	39, 40	3.25	3.11	8.0	8.1	8.8	50.5	15.8	1.63	−2.5	50	2.0	1.2	68	43	2, 3, 4
Lava Mtn	51	3.80	3.83	8.1	8.3	8.2	51.4	16.2	1.80		55	2.3	1.7	74	56	5
Big Pine	37	3.72	2.93	8.9	8.5	12.0	48.0	16.7	1.77	−1.9	74	2.0	1.3	68	46	2, 3, 4
DV-PP-Owens	13, 36	3.30	3.27	8.9	9.1	8.2	49.4	16.3	1.75	−3.0	85	2.7	1.9	90	64	6
Coso	35	2.94	2.84	9.2	9.4	8.6	48.1	17.7			93	2.8	1.8	93	61	7
Mina	41	3.30	3.28	8.8	9.4	9.0	49.2	16.6	1.51	−1.4	98	2.8	2.1	92	70	2, 3, 4
Long Valley	39, 40	3.30	3.35	8.0	7.8	7.6	50.0	16.0	1.74	−4.8	99	2.0	1.2	68	43	2, 3, 4
Saline Range 1	11	3.57	3.32	10.3	10.4	10.0	48.2	16.9		−4.0	100	3.5	3.1	115	102	8
Saline Range 2	11	3.70	3.77	9.6	9.5	9.3	48.2	17.0		−3.1	100	3.0	2.5	99	83	8
Pisgah	46	3.70	3.72	10.1	10.4	8.2	47.5	15.7	1.69	4.0	116	3.6	3.2	117	103	9
Pinto Peak	12	3.28	2.67	9.4	10.3	13.7	48.9	16.3	1.52	−0.4	118	3.1	2.4	102	80	10
SW border NV	4, 7	3.30	3.19	8.7	9.4	9.5	49.2	15.9	1.70	−6.0	141	2.8	2.1	92	70	6
Amboy	47	3.63	3.62	10.1	10.2	8.6	47.3	15.2	1.65	4.6	151	3.5	3.0	113	97	9, 11
Cima (<1Ma)	14	3.36	3.28	10.6	10.7	8.2	49.1	15.4	1.82	8.3	188	3.8	3.1	121	101	12
Cima(>3Ma)	14	3.00	2.91	10.7	10.8	8.2	47.2	15.7	1.73	7.1	188	3.8	3.0	123	98	12
Crater Flat	7, 8	3.18	3.10	11.3	11.5	9.0	47.2	15.4	2.17	−5.7	196	4.1	3.5	133	115	13, 29
Test site	5, 7	3.36	3.20	9.9	9.9	9.0	48.4	16.4	1.70	−5.8	217	3.3	2.7	106	87	1, 5, 12
Reveille Range	3	3.50	3.60	11.7	11.6	8.3	44.6	15.1	1.96	3.2	290	4.3	3.9	139	126	14
Lake Mead	27, 29, 31, 33	3.30	3.14	12.4	12.8	9.0	45.9	14.8		2.4	303	4.9	4.4	158	140	5, 15, 16
Lava Cascade	26, 27	2.73	2.82	11.4	11.9	9.0	44.6	15.2		1.8	309	4.4	3.5	142	114	5, 15, 16
Fortification	29	2.92	2.92	11.4	11.4	8.0	46.3	13.7		−0.8	310	4.3	3.4	137	110	5
Petroglyph Wash	27, 30	2.89	2.88	11.3	11.5	9.0	47.5	14.6		−0.4	318	4.2	3.4	135	110	5
Lunar Crater	1	3.47	3.44	12.4	12.8	8.9	46.4	15.1	1.90	5.3	321	5.0	4.8	162	155	5, 17, 28
Gold butte	31	3.10	3.06	11.0	11.1	9.2	46.1	14.9		−1.2	354	3.9	3.2	127	105	5, 18
EST gap	28	3.10	3.00	11.5	11.7	8.8	46.5	15.0		−7.0	383	4.3	3.6	140	118	5, 18
Pakoon Springs	54	3.04	2.89	11.2	11.7	8.7	46.5	14.6			386	4.3	3.6	139	117	5, 18
Mud Mountain	28	3.60	3.52	11.6	11.8	8.4	47.3	14.7		3.4	411	4.4	3.7	143	121	5, 18
Gunlock	SW UT	3.55	3.48	9.8	10.1	9.0	49.4	16.1			442	3.3	2.8	109	93	19
West Grand Canyon	48, 49, 50	3.33	3.10	11.0	12.0	10.0	48.6	15.1	1.83	1.0	443	4.3	3.7	140	121	20
Diamond Valley	SW UT	3.20	3.15	11.4	11.8	8.3	48.6	15.4			449	4.5	3.9	144	125	21
Hur (alkali basalts)	10	3.30	3.35	10.5	10.7	8.6	48.5	15.7	1.58	−0.2	468	3.7	3.1	120	101	22
Hur (basanite)	10	2.78	2.88	10.9	11.6	11.8	48.8	14.4	2.77	−2.6	474	4.1	3.4	131	109	22
Hur (low Nd)	10	2.82	2.76	10.6	10.9	8.5	50.0	15.1	2.00	−7.4	474	3.8	2.9	123	95	22
SVF	32	3.10	3.04	10.1	10.4	9.3	47.6	15.1			528	3.4	2.7	112	90	23, 24
Geronimo	SE AZ	3.97	3.77	10.1	9.9	9.0	46.3	16.1	1.57	7.1	530	3.3	3.0	108	98	25
Sunset Crater	32	3.19	3.09	10.5	10.2	8.8	47.0	15.5	1.70	0.7	532	3.4	2.7	112	90	26
Markagunt	52	3.35	3.69	9.3	8.9	9.3	50.2	15.7	1.56	−5.5	533	2.6	1.9	84	62	27

[a]Major element compositions are at 8.0 wt % MgO and "primitive" values, as in Figure 3. Tb/Yb values are basalt averages, normalized to chondritic values by *Sun and McDonough* [1989]. Location and distance from A along the reference line from Figure 1. Initial pressure P_o and final pressure P_f of melting calculated from primary values after adding olivine and using the melting model of *Langmuir et al.* [1992]. Depth Z calculated from pressure, and crustal thickness and density given in Figure 7. Epsilon(Nd) is average of basalts only (<52% SiO2).

[b]References: 1, *Feldstein and Lange* [1999]; 2, *Ormerod et al.* [1988]; 3, *Ormerod et al.* [1991]; 4, *Rogers et al.* [1995]; 5, CVTS (unpublished data) (available at http://www.unlv.edu/Research_Centers/Volcanic_and_Tectonic_Studies/tech_pub.html; this link points to a large list of technical publications by CVTS in the last two decades, including journal papers, technical reports, M.S. theses, and others); 6, *Ormerod* [1988]; 7, *Babcock* [1977]; 8, *Hoffine* [1993]; 9, *Glazner et al.* [1991]; 10, *Coleman and Walker* [1990]; 11, *Glazner et al.* [1991]; 12, *Farmer et al.* [1995]; 13, *Bradshaw and Smith* [1994]; 14, *Yogodzinski et al.* [1996]; 15, *Feuerbach et al.* [1993]; 16, *Feuerbach* [1998]; 17, *Lum et al.* [1989]; 18, *Cole* [1989]; 19, *Embree* [1970]; 20, *Wenrich et al.* [1995]; 21, *Nusbaum et al.* [1995]; 22, *Smith et al.* [1999b]; 23, *Alibert et al.* [1986]; 24, *Wilshire et al.* [1988]; 25, *Kempton et al.* [1987]; 26, *Blaylock et al.* [1996]; 27, *Nealey et al.* [1997]; 28, *Bergman* [1982]; 29, *Vaniman et al.* [1982].

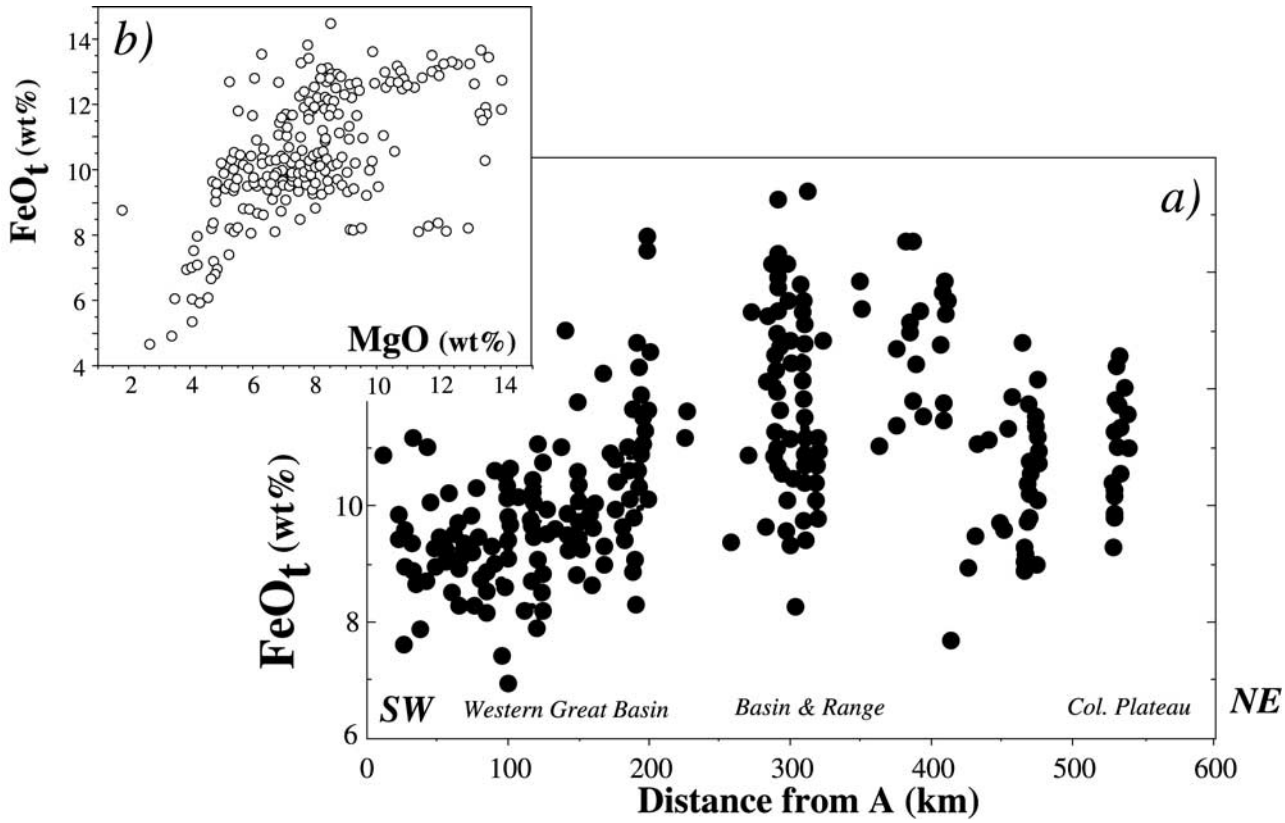

Figure 2. (a) FeO(total) in basalts (SiO_2 < 52%) versus distance from the reference point A in Figure 1. All basalts plotted are younger than 8.5 Myr. Data sources are given in Table 1. Note the low FeO_t concentrations in basalts from the Western Great Basin and high FeO_t in basalts from the Central Basin and Range. (b) Inset showing FeO(total) versus MgO for basalt groups from late Cenozoic volcanic fields in southern Nevada and adjacent regions. Note the preponderance of samples with MgO of 6–9 wt %.

Tectonic Studies (CVTS) at the University of Nevada, Las Vegas (for chemistry), and the Isotope Geochemistry Laboratory (IGL) in the Department of Geology at the University of Kansas (for isotopes) over the past 10 years. About 20 of these samples either lacked trace element data or had trace element data with poor precision and were reanalyzed at the Plasma Analytical Laboratory in the Department of Geology at the University of Kansas (KU-PAL) using an inductively coupled plasma mass spectrometer. An additional six samples were analyzed at KU-PAL for major element chemistry using an inductively coupled plasma atomic emission spectrometer. Analytical procedures are given by *Johnson and Plank* [2000] and *Feuerbach et al.* [1993].

[8] These data were compiled along with ~600 additional published analyses from southern Nevada and adjacent areas (compilation will be made available by K. Wang et al., manuscript in preparation). The majority of samples have fairly complete geographic, temporal, and compositional data, including latitude, longitude, age, Pb, Sr, and Nd isotopic ratios, 10 major elements, and 28 trace elements. The locations of samples from many of the earlier studies are estimated from geologic maps, whereas most samples from CVTS and IGL have fairly precise latitudinal and longitudinal data. To make the data set internally consistent, all the data are recalculated H_2O free, with Fe expressed as total FeO (FeO_t).

[9] Undoubtedly, there exist systematic biases between different laboratories in the determination of major and trace element concentrations because the data were compiled from diverse sources with analytical work done over the past 30 years. Although no attempt was made for correcting those biases, they are not a major source of uncertainty because almost half of the major and trace element data in our data set were from CVTS/IGL. Conclusions made in this paper do not differ on the basis of using the full data set or only the CVTS/IGL sample set.

[10] All basalts considered are younger than 8.5 Myr except for those from Gold Butte (9 and 9.5 Myr). There is no compelling evidence that regional systematics in 0–4 Myr basalts are significantly different from those in 4–8.5 Myr (although in some regions there may be local temporal systematics). Thus all B&R basalts <10 Myr are included in this study, and all results presented are age-averaged over the last 10 Myr.

3. Major Element Variations in Basalts Across the Basin and Range

[11] Because our melting model is primarily based on major element compositions, it is useful first to consider the variations observed in basalts across the B&R province. In order to simplify our examination of regional patterns, data are projected onto a line parallel to the direction of previous subduction and crossing the middle of the study region (A-A′ in Figure 1). Distance from A along the transect is given for each volcanic field in Table 1. This projection juxtaposes volcanic fields that are very far apart (e.g., Lunar Crater and Lake Mead) and may lie within the physiographically distinct northern, central, and southern B&R. Nonetheless, the projection is useful in illustrating some major differences in basalt chemistry and lithospheric thickness across the study area. Some chemical differences (FeO) are highlighted in Figure 1 to illustrate the map pattern of variation.

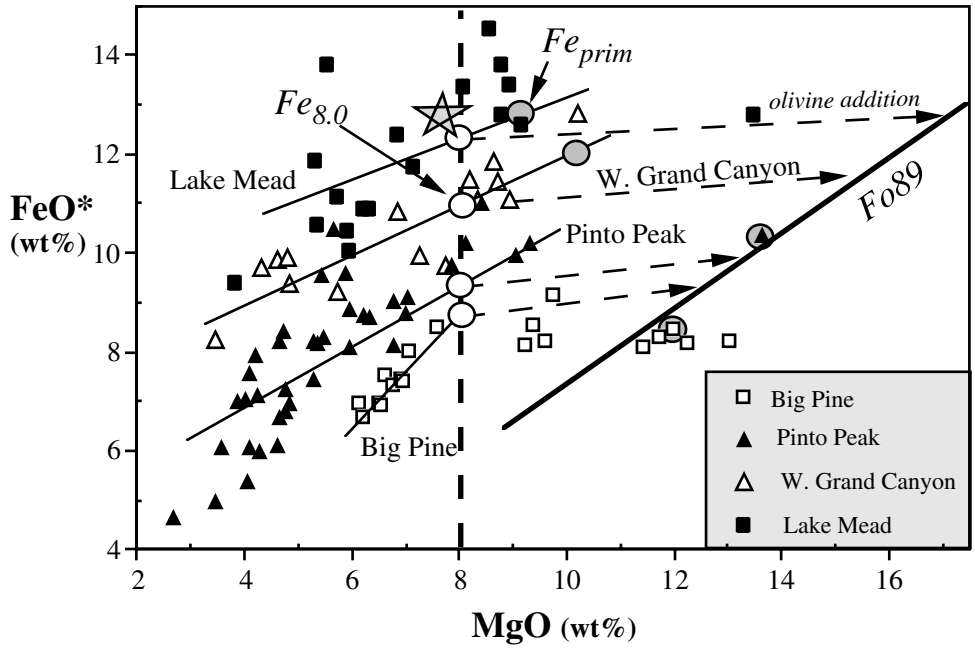

Figure 3. Examples of fractionation-correction schemes for FeO (total). $Fe_{8.0}$ (open circle) is the FeO concentration at 8% MgO and is calculated from regression lines for each group (thin solid lines). Fe_{prim} (shaded circle) is the most primitive FeO concentration for each group, based on the most MgO-rich samples that lie near or on the regression line. $Fe_{8.0}$ and Fe_{prim} compositions are then extrapolated to primary ones by adding olivine (dashed lines) until compositions are in equilibrium with Fo_{89} in the mantle (thickest line). These four groups encompass nearly the entire range in $Fe_{8.0}$ for basalts from the study region (see Table 1 for all values and references). The star is the average of Snake River basalts [*Lum et al.*, 1989].

[12] Figure 2a shows variations of FeO_t across the B&R for all the basalts (SiO_2 < 52 wt %) younger than 8.5 Myr. FeO_t shows a clear trend, increasing from west to east to the middle of the profile and then decreasing farther eastward. A similar but inverse trend is observed for SiO_2. As mentioned previously, the difference in SiO_2 contents of basalts between the WGB and B&R was also noted by *Rogers et al.* [1995], who interpreted the variations as reflecting changes in the depth of melting.

[13] There are two possible causes of the trends observed. One includes processes that occur after magma generation (fractional crystallization and/or contamination), whereas the other includes processes that occur during or prior to magma generation (differences in the melting depth, mantle composition, and/or degree of partial melting to form primary magma). Although some workers report crustal contamination in B&R basalts [*Walker and Coleman*, 1991; *Glazner and Farmer*, 1992; *Yogodzinski et al.*, 1996], others [*Fitton et al.*, 1991; *Kempton et al.*, 1991; *Fraser et al.*, 1985; *Perry et al.*, 1987; *Fitton et al.*, 1988; *Ormerod et al.*, 1988; *Leat et al.*, 1988; *Lum et al.*, 1989; *Reid and Ramos*, 1996; *Menzies et al.*, 1983; *Beard and Johnson*, 1997; *DePaolo and Daley*, 2000] suggest that in many cases isotopic compositions of continental basalts still reflect variation in the mantle source. Thus isotopic and geochemical compositions of basalts from the B&R have been used to study mantle chemical characteristics [*Daley and DePaolo*, 1992; *Feuerbach et al.*, 1993; *Bradshaw et al.*, 1993; *Farmer et al.*, 1989, 1995; *Rogers et al.*, 1995; *Cooper and Hart*, 1990; *Livaccari and Perry*, 1993; *Smith et al.*, 1999b; *Menzies et al.*, 1985; *Ormerod et al.*, 1991]. In a companion paper (K. Wang et al., manuscript in preparation), we also attempt to quantify crustal contributions (using $^{143}Nd/^{144}Nd$ and Nb/Ba variations with SiO_2) and conclude that most volcanic centers preserve vestiges of mantle signatures when projected to basaltic compositions (<52 wt% SiO_2). Thus it is important to correct first for variations caused by secondary processes before we can isolate primary ones caused by the melting process.

3.1. Correcting for Crustal Differentiation

[14] With some notable exceptions (basalts from Big Pine and Geronimo [*Rogers et al.*, 1995]), few B&R basalts may be considered primary. Thus, at a minimum we must first correct for the effects of fractional crystallization on the major element variations for different lava suites. One approach is to project all the basalt data to a high MgO value, closer to primary compositions [e.g., *Klein and Langmuir*, 1987; *Plank and Langmuir*, 1988]. Given the preponderance of compositions between 6 and 9 wt % MgO in B&R basalts (Figure 2b), we project compositions to 8 wt % MgO. Most volcanic suites include some compositions $\geq$ 8 wt % MgO; projecting to higher MgO (e.g., 9 wt %), however, would limit significantly the number of volcanic centers that could be considered. Figure 3 illustrates the $Fe_{8.0}$ calculation, where $Fe_{8.0}$ is the FeO_t value on the regression line at 8 wt % MgO. An uncertainty (Fe_8-err in Table 1) is calculated using the error envelope of *Till* [1974] for each volcanic group. This uncertainty may reflect real differences in primary magmas or scatter in the data produced by crystal fractionation. This correction method is similar to that used by *Plank and Langmuir* [1988], where the empirical trends in the data are assumed to represent segments of liquid lines of descent (LLDs). In a continental setting, LLDs are complex and will vary locally depending on the magnitude of local assimilation-fractional crystallization (AFC) processes. By using the data trends themselves, we are making no a priori assumptions about the causes of magma evolution but simply correcting for them. In this way the correction differs from that used to calculate $Fe_{8.0}$ in MORB, where a theoretical LLD slope was used [*Klein and Langmuir*, 1987]. The only assumption we are making to correct the B&R basalts is that secondary processes are minimized and primary processes are better revealed at high MgO (i.e., 8 wt %).

[15] It is possible that the above correction scheme introduces biases brought about by variable AFC processes or LLDs, and so we adopt a second approach using only the most primitive samples from each individual volcanic field. We develop Fe_{prim} values that represent the most primitive FeO_t concentrations for each group and are based on the highest MgO samples that lie near the regression lines (Table 1). The advantage of this method is that it requires little treatment of the data; the disadvantage, however, is that the primitive samples from different volcanic fields will represent different degrees of fractional crystallization and/or contamination. Because there are advantages and disadvantages to both approaches, we calculate primary liquids using both $Fe_{8.0}$ and Fe_{prim}. In general, the compositions at 8% MgO are best for comparing compositions across the B&R, while the most primitive compositions are best for use in the quantitative melting model. We consider below the effect of using $Fe_{8.0}$ versus Fe_{prim} to quantify melting depth.

[16] Figure 3 shows similar slopes for data arrays among several representative suites of volcanic rocks. None are consistent, however, with theoretical low-pressure crystallization of olivine, plagioclase, and clinopyroxene (the main observed phases), which should lead to FeO enrichment [e.g., *Langmuir et al.*, 1992]. The FeO depletion trends observed may require either a lack of plagioclase separation, magnetite in the fractionating assemblage, or crustal contamination. Regardless of the exact cause in each case, the AFC processes will be minimized by projecting to MgO = 8%. Because of the FeO depletion trends, $Fe_{8.0}$ values provide a minimum estimate of both primary FeO and calculated melting depths. Above 8–9% MgO, however, the FeO content in most magma suites is constant or decreases slightly with increasing MgO. This is characteristic of olivine crystallization and so is fairly straightforward to correct. Below, we will use an olivine-addition method to correct for olivine fractional crystallization above 8% MgO and extrapolate to primary compositions in equilibrium with mantle olivine (Fo_{89}).

[17] For some volcanic areas, too few data are available for a particular center to form a significant regression. For those areas, data are grouped with those from adjacent centers. In general, we try to group those adjacent areas where samples tend to form a single trend. We interpret this to mean that the volcanic rocks in one group very likely derive from a similar parental magma. Thus the melting results obtained will be averages for those areas. In other areas, data are sufficient to separate samples into different groups according to rock type and/or age (e.g., Hurricane and Cima, Table 1). In these cases we are able to interpret whether different rock series derive from different melting conditions.

[18] For a specific volcanic center or group of basalts, if all the samples have MgO far above or below 8%, they are excluded from the $Fe_{8.0}$ calculation. For example, all the alkali basanites in the Hurricane volcanic field have MgO >13%, and the linear relationship between MgO and FeO and/or SiO_2 is poor, so extrapolation back to MgO = 8% is poorly constrained. On the other end of the spectrum, all of the Crater Flat basalts form a cluster at <5.5 wt % MgO, and so they are combined with nearby areas to regress a line.

[19] Basalts from some volcanic fields (e.g., Pinto Peak, Pisgah, and Amboy) show strong evidence for crustal contamination [*Walker and Coleman*, 1991; *Glazner et al.*, 1991]. Nonetheless, since these fields still include very mafic compositions (>8 wt % MgO; Figure 3), not all samples have been extensively contaminated, and we maintain that projection to high MgO maximizes precontamination characteristics. We correct these basalts the same way as for other uncontaminated samples and find that depth calculations based on $Fe_{8.0}$, $Na_{8.0}$, and Tb/Yb conform well to those for nearby centers as well as the regional trend.

3.2. Variations at 8 wt % MgO in Basin and Range Basalts

[20] Values and ranges of Fe_8, Na_8, Si_8, and average Tb/Yb for 40 groups of basalts from the study region are listed in Table 1 (Tb/Yb are basalt averages; no fractionation correction is applied since incompatible trace element ratios are relatively insensitive to the effects of crystal fractionation). Figure 4 shows the variation of $Fe_{8.0}$, $Si_{8.0}$, $Al_{8.0}$, and Tb/Yb across the B&R. There is clearly a systematic relationship among these elements, where $Fe_{8.0}$ correlates inversely with both $Si_{8.0}$ and $Al_{8.0}$. These variations are precisely those expected for mantle melts derived from different depths of melting, where higher pressure melts will have higher Fe but lower Si and Al [e.g., *Langmuir et al.*, 1992; *Hirose and Kushiro*, 1993]. Tb/Yb increases from the southwest to the northeast, reaching maximum values in the Central B&R in the middle of the profile, before decreasing somewhat toward the Colorado Plateau. Note that $Fe_{8.0}$ shows the same overall trend that was apparent in the uncorrected data (Figure 2a).

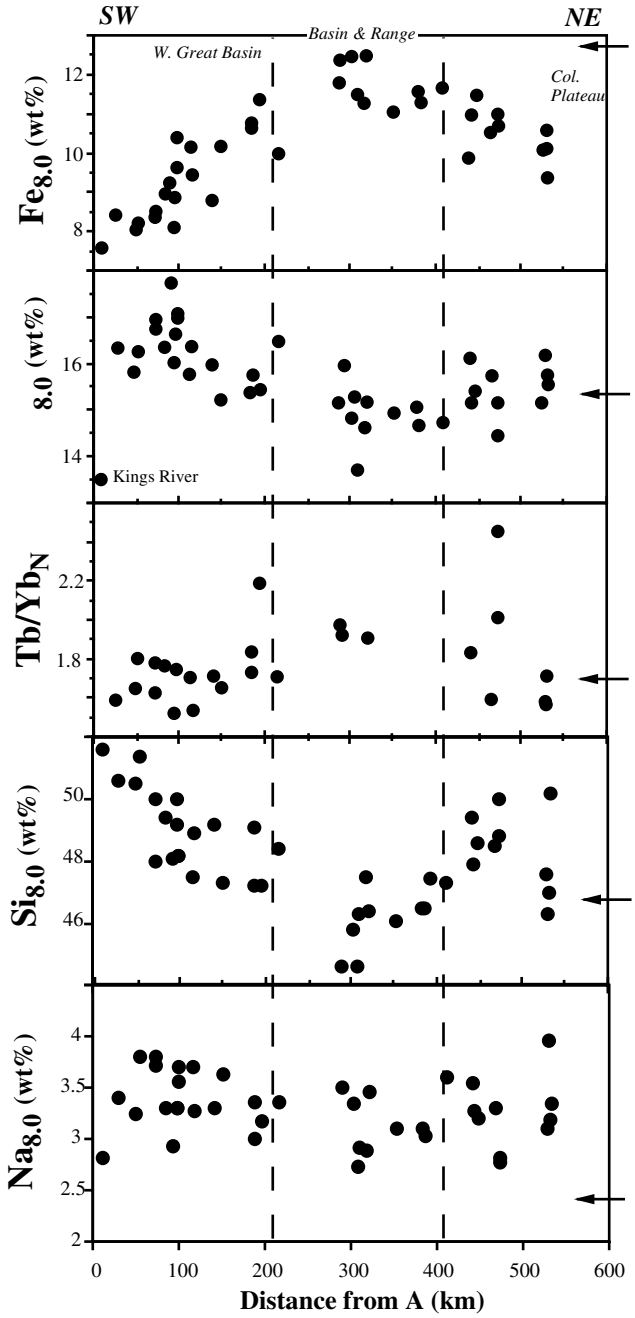

Figure 4. Systematic variations of fractionation-corrected major and trace elements in basalt groups across the Basin and Range province (distance from A as in Figure 1). The arrow shows average Snake River basalt [from *Lum et al.*, 1989].

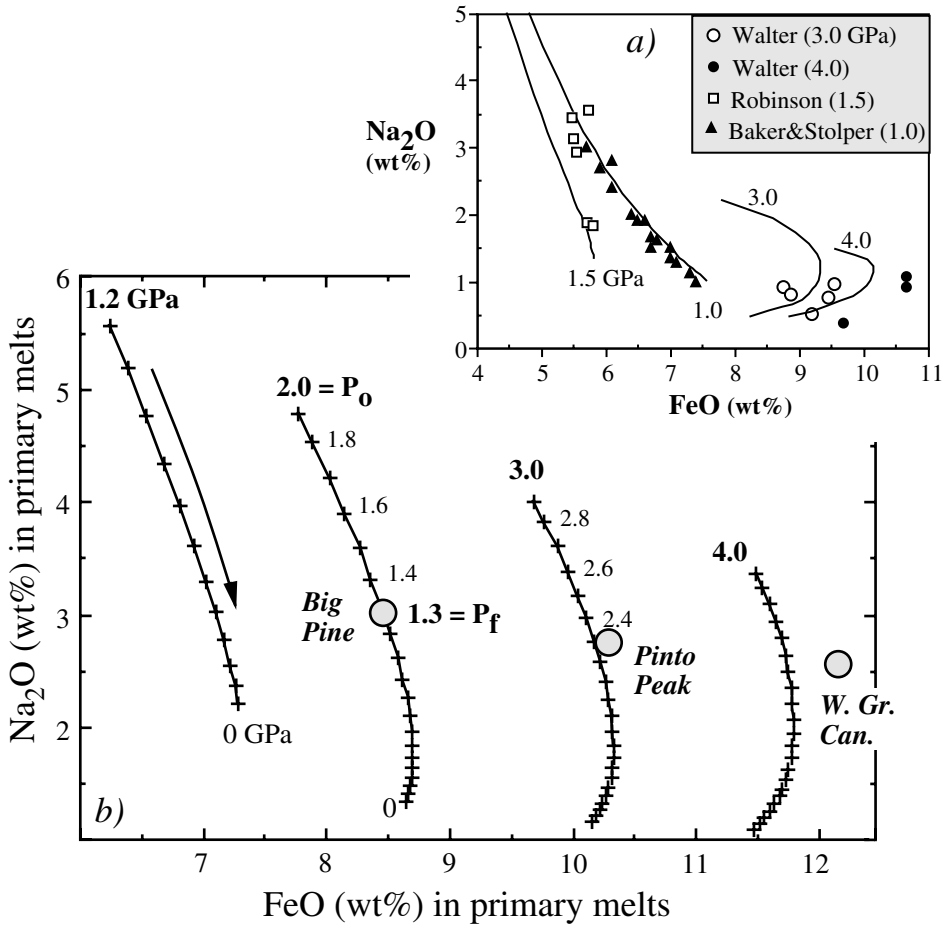

Figure 5. (a) Comparison between melting model (lines) and experimentally determined peridotite melts (symbols). The melting model, after *Langmuir et al.* [1992], is "tuned" for each set of experiments by inputting starting composition, pressure, solidus T, and dT/dF. Melting models and experimental data are isobaric (P indicated). Experimental data are from *Walter* [1998], *Robinson et al.* [1998], and *Baker and Stolper* [1994]. Note that the 1.5 GPa curve has lower FeO than the 1.0 GPa curve owing to the low FeO starting composition used by *Robinson et al.* [1998]. (b) Examples of how melting model is used to estimate pressures of melting for Basin and Range basalts. Lines are polybaric mantle melting paths during adiabatic decompression [after *Langmuir et al.*, 1992]. Each tick mark represents 0.1 GPa (1 kbar) of decompression, after which fractional melts are accumulated to give primary FeO and Na_2O contents. The arrow shows direction of melting, from the pressure of intersection of the solidus (P_o) to the surface ($P = 0$). Large shaded dots are primary melt compositions for each region, calculated by adding olivine to Fe_{prim} and Na_{prim} averages (see Table 1 and Figure 3) until melts are in equilibirum with Fo_{89}. The FeO and Na_2O content of the Basin and Range basalt averages gives a unique P_o and P_f (final pressure) for each region (actual values given in Table 1).

[21] In order to preserve a negative Fe-Al correlation (Figure 4) that reflects varying pressure of melting, olivine must be the major fractionating mineral for the parent magma of the basalts. A theoretical simulation of fractional crystallization using published primary magmas [*Hirose and Kushiro*, 1993] and an LLD program [*Weaver and Langmuir*, 1990] indicates that early plagioclase crystallization (i.e., when MgO > 8%) would disrupt the $Fe_{8.0}$-$Al_{8.0}$ correlation and that early high-pressure clinopyroxene crystallization would produce a positive $Fe_{8.0}$-$Al_{8.0}$ trend. In general, the simulation supports our earlier assumption that the primitive lavas are dominated by olivine fractionation, and AFC processes mainly occurred at <8% MgO.

4. Mantle Melting Model

[22] We use the model developed by *Langmuir et al.* [1992] (LKP model) to quantify the pressure and degree of mantle melting. The LKP model describes compositional changes (FeO, MgO, and Na_2O) in mantle melts during adiabatic decompression, assuming olivine-melt equilibrium and trace element behavior for Na. Unlike other melting models, which are parameterized for and therefore dependent on the limited data set of multiply saturated peridotite melts, the LKP model is based simply on the partition coefficients (K_d) for Mg and Fe in olivine, which are well constrained from hundreds of experiments. The MgO and FeO concentrations in peridotite melts are imposed by olivine saturation and can be calculated robustly from K_d expressions (which are themselves a function of P, T, and alkali content). Na_2O is calculated from its K_d in clinopyroxene (which is also P and T dependent) and using a nonmodal trace element melting equation (see *Langmuir et al.* [1992, Appendices A and B] for all expressions used). Other inputs to the model include the initial composition of the mantle (MgO, FeO, Na_2O, and %clinopyroxene), the mantle solidus, and the relationship between T and F (% of melting) during isobaric and adiabatic melting.

[23] Although the LKP model was developed for mid-ocean ridge basalts, it is a general model for dry melting of the mantle and reproduces well the systematics in recent peridotite melting experiments conducted between 1.0 and 4.0 GPa [e.g., *Baker and Stolper*, 1994; *Robinson et al.*, 1998; *Walter*, 1998] (Figure 5a). None of the data in these more recent experiments were used to calibrate the LKP model, and so this is an independent test of the model. Figure 5a shows how the melting model mimics trends in the experiments, both as a function of increasing melt fraction (decreasing Na_2O) within each experimental dataset and as a function of increasing pressure (increasing FeO generally) between each experimental study. The agreement with the experiments of *Baker and Stolper* [1994] is particularly impressive (Figure 5). The model appears to underestimate FeO at high pressure, on the basis of the mismatch with Walter's experiments at 4.0 GPa. This may lead to an overestimation of melting depths at >110 km. The results of this study, however, predict most melting within the interval between 50 and 110 km, where the model is well constrained.

[24] The flexibility in input parameters in the LKP model permits us to consider different mantle source compositions for the continental mantle. Mantle source concentrations for major elements will vary naturally as a function of peridotite fertility. Figure 6 shows a compilation of peridotite xenolith data from across the B&R. Na_2O and MgO vary simply with clinopyroxene content, from low-Na_2O, high-MgO depleted harzburgites (at <5% clinopyroxene) to high-Na, low-Mg fertile lherzolites. Although most of these peridotites have undergone a complex history [e.g., *Smith et al.*, 1999a; *McGuire and Mukasa*, 1997], the major element variations conform generally to those expected for melt removal processes. Aside from some unusual harzburgites that have experienced Fe enrichment, most peridotites have relatively constant FeO at 7.5–8.5 wt % (Figure 6). For our initial modeling we use an average fertile lherzolite composition with 15% clinopyroxene (MgO = 39.5%, FeO = 8.2%, Na_2O = 0.29%, Mg # = 89.5). This composition is very similar to estimates of primitive mantle [*Hofmann*, 1988] or "normal" fertile mantle (LKP) and is identical to the average olivine composition in B&R mantle xenoliths [*Smith*, 2000]. Uncertainties resulting from varying source concentrations will be discussed below.

[25] The LKP model also allows for different mechanisms of melt pooling along the adiabatic ascent path and for different melting regime shapes [*Plank and Langmuir*, 1992]. There are two extreme models for melt pooling: batch melting and fractional melting. After the mantle rises above its solidus P_o, melt may be extracted instantaneously (pure fractional melting) or remain in equilibrium with the residue up to the depth where upwelling and melting stop (P_f, batch melting). We consider pure fractional or pure batch melting unlikely and prefer accumulated fractional melting, which results in melt compositions between batch and fractional melts [*Langmuir et al.*, 1992]. In the model used, melt is pooled after each kbar (0.1 GPa) of P release. Melt productivity decreases along the melting path and ranges from 0.9 to 1.4%/kbar for the range of pressures explored here. If the melting rate is substantially lower [*Asimow et al.*, 1995], then calculated melting columns will be longer to achieve the same amount of melting (and Na_2O contents), but the relative differences between melting columns would remain. We assume simple one-dimensional (1-D) upwelling paths (a melting column); without better constraints on the geometry of upwelling and melting in the B&R, there is no point in considering more complex 2-D or 3-D melting regime shapes. For magma with Na_2O > 3.0 (relevant to the B&R), batch melting and accumulated fractional melting curves converge [see *Langmuir et al.*, 1992, Figure 46a], and so our results are not highly sensitive to the selection of the melt pooling mechanism.

[26] Accumulated fractional melting paths generated by the LKP model are shown in Figure 5b for primary Fe and Na. Each curve represents a different pressure of intersection with the mantle solidus P_o, from 1.2 to 4.0 GPa. P_o will increase with increasing mantle potential temperature [*McKenzie and Bickle*, 1988]. As the mantle ascends above the solidus, the total melt fraction F increases until the pressure where the mantle ceases to ascend adiabatically (P_f) and therefore ceases to melt. The total melting column length ($P_o - P_f$) thus determines F. Increasing F has the main effect of lowering Na_2O in the melt, as Na_2O behaves as an incompatible element that is diluted by further increments of melting. The bulk partition coefficient for Na (D) varies as a function of temperature, pressure, and clinopyroxene in the residue

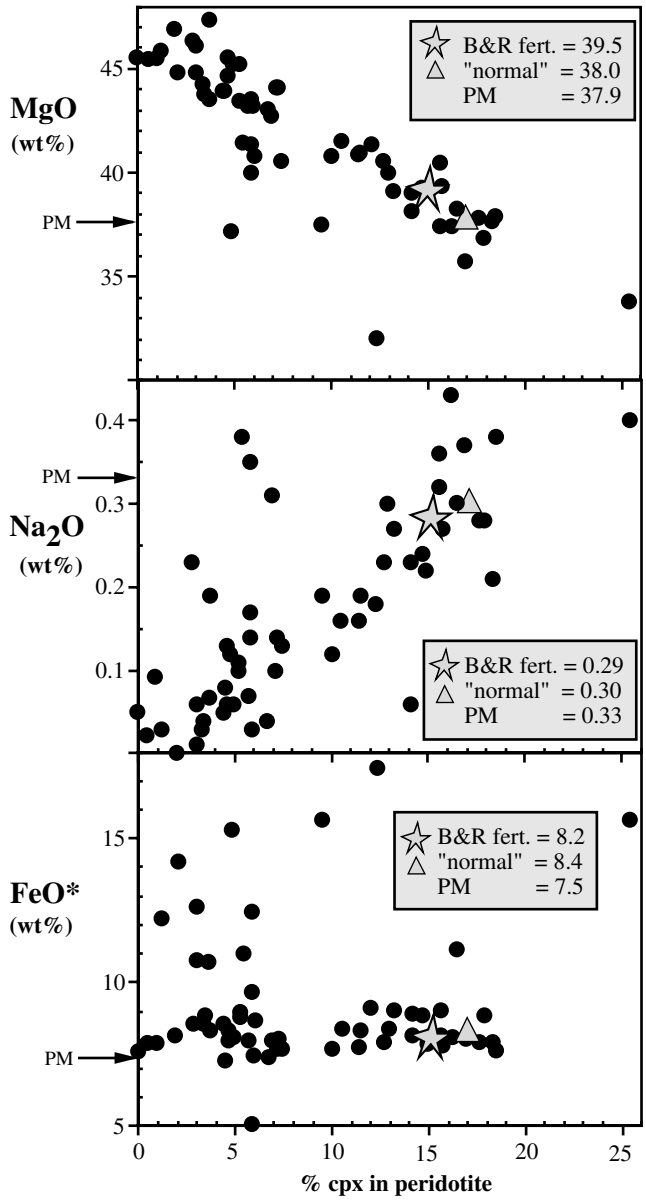

Figure 6. Peridotite xenoliths across the Basin and Range and into the Colorado Plateau transition zone [*Wilshire et al.*, 1988; *McGuire and Mukasa*, 1997; *Smith et al.*, 1999a; *Beard and Glazner*, 1995; *Frey and Prinz*, 1978]. Average Basin and Range fertile lherzolite mantle composition is shown as a star, corresponding to ~15% clinopyroxene (cpx) in the peridotite and Mg # = 89.6. Primitive mantle (PM) [from *Hofmann*, 1988] and "normal" fertile mantle (triangle) [from *Langmuir et al.*, 1992] are shown for comparison. Cpx percent is either from published mode or calculated from whole rock CaO and published microprobe cpx CaO or assuming 21 wt % CaO in cpx.

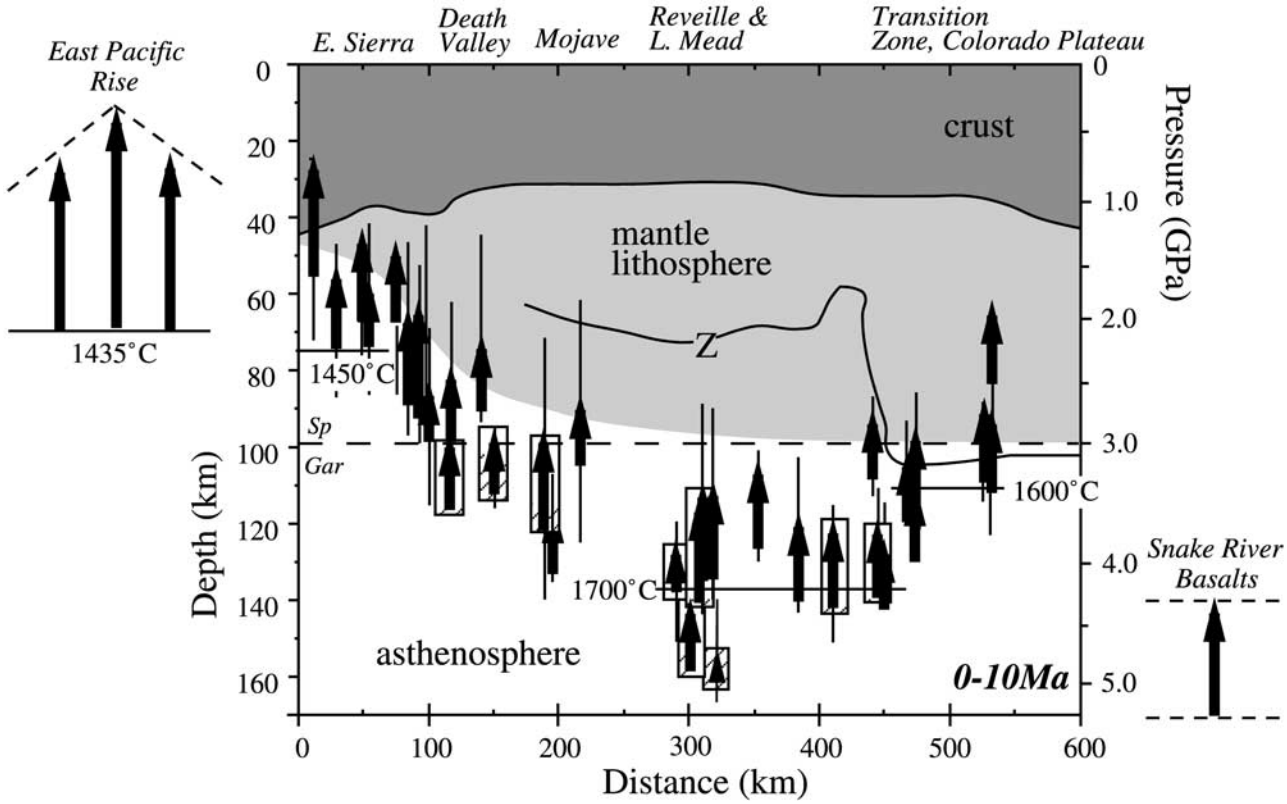

Figure 7. Melting profile across the Basin and Range (distance from A, as in Figure 1). The arrow represents the melting column calculated for each volcanic field (Table 1), based on the most primitive FeO and Na_2O compositions. The bottom of the arrow marks the onset of melting at the solidus and is a function of mantle temperature, while the top of the arrow marks the end of decompression melting, presumably due to the change in rheology near the lithosphere-asthenosphere boundary. The thin line extensions to the arrows include depth estimates and errors using $Fe_{8.0}$. Crustal thickness was compiled from *Das and Nolet* [1998]. Shaded lithosphere is based on lithosphere thickness (L_m + Moho) estimates of *Jones et al.* [1996], which were averaged and smoothed for the Sierras, Central and Southern Basin and Range, and western edge of the Colorado Plateau. Estimates for the Northern Basin and Range were not used owing to negative L_m values; thus there is a lack of control from 300 to 500 km. The shape of the lithosphere is consistent with the conceptual model of *Wernicke* [1992]. Alternative boundary for the base of the lithosphere (marked with a *Z*) is based on *P* wave residuals from *Zandt et al.* [1995], although this model does not take into account mantle *T* or compositional effects on seismic velocity. The spinel-garnet transition in peridotite is after *Klemme and O'Neill* [2000] and *Robinson and Wood* [1998]. Ruled bars are for melting columns with average ε_{Nd} of > +0.5. Melting depths for the Snake River basalts shown for reference (average of data from *Lum et al.* [1989]). The East Pacific Rise shows analogous melting calculation for primitive MORB near the Tamayo Fracture Zone [*Bender et al.*, 1984], assuming melt pooling from a triangular-shaped melting regime [*Plank and Langmuir*, 1992]. Temperatures given are solidus temperatures of adiabatically ascending mantle. The pressure axis was calculated assuming 35 km crust with 2.85 g/cm^3 density overlying mantle of 3.25 g/cm^3 density.

and therefore varies during melting from 0.07 at high P_o (4.0 GPa) on the solidus with 15% cpx in the residue to 0 at the point of cpx exhaustion. On the other hand, FeO varies largely as a function of P_o, with relatively small variations as a function of *F*. The increase in FeO with increasing pressure is largely due to the effect of temperature on olivine K_d and the dominating effect of increasing temperature as pressure increases along the mantle solidus [*Langmuir et al.*, 1992]. Thus the final Na and Fe contents of mantle melts provide excellent constraints on the initial depth of melting (from FeO, which reflects P_o), and the final depth of melting (from Na_2O, which reflects *F* and therefore $P_o - P_f$). In theory, deriving the depth of melting is thus a simple matter of plotting primitive basalt compositions on Figure 5b.

[27] In order to compare quantitatively the B&R basalt data to the primary melt compositions from the model output, the basalt data must be extrapolated to primary compositions. We use an olivine-addition method to extrapolate both the fractionation-corrected data (at 8% MgO) and the most primitive basalt samples. Equilibrium olivine is added in 1% increments until the resulting basaltic magma is in equilibrium with Fo_{89} olivine (similar to the average B&R xenolith olivine, $Fo_{89.6}$ [*Smith*, 2000]), using K_D = 0.3, where K_D is the molar ratio of FeO/MgO in olivine to that in the coexisting magma. $Na_{8.0}$ and Na_{prim} are diluted according to the amount of olivine added.

[28] Inversions for melting parameters were carried out for both the olivine-corrected $Fe_{8.0}$-$Na_{8.0}$ and Fe_{prim}-Na_{prim} (Table 1 lists results based on most primitive compositions only). For example, basalts of the Big Pine volcanic field require that melting start at $P_o \sim 2.0$ GPa and stop at $P_f \sim 1.3$ GPa, for ~8.8% total melting (Figure 5b). We obtained P_o and P_f for all 40 groups of basalts in this way (Table 1, Figure 7). To convert pressure to depth, densities of crust and mantle are assumed to be 2.85 g/cm^3 and 3.25 g/cm^3, respectively [*Jones et al.*, 1992]. Crustal thickness for each volcanic field is approximated from the crustal thickness map of *Das and Nolet* [1998]. Changing crustal density from 2.85 to 2.65 g/cm^3 would result in <1 km difference in estimated melting

depths. Table 1 gives depths to the bottom (Z_o) and top (Z_f) of the melting column, as calculated from Fe_{prim} and Na_{prim}.

[29] In accord with the qualitative results from $Fe_{8.0}$, $Al_{8.0}$, $Si_{8.0}$, and Tb/Yb, the results from the melting model indicate that the melting depth increases along the profile northeastward in the first 300 km (East Sierra-Death Valley-Mojave), reaching a maximum in the central B&R before decreasing gradually toward the Transition Zone to the Colorado Plateau (Figure 7). All the melting columns are shallower than 140–160 km depth, and most fall between 50 and 130 km, with an average of ~100 km (Figure 7). Along the profile, the top of our melting regime generally follows the mantle asthenosphere-lithosphere boundary inferred from independent geological and geophysical constraints [*Wernicke*, 1992; *Jones et al.*, 1992; *Wernicke et al.*, 1996] (see section 5.1). This makes sense, as the mantle lithosphere should provide a lid to asthenospheric upwelling and melting. The deepest melting columns also appear to coincide with the highest $^{143}Nd/^{144}Nd$ (or ε_{Nd}) basalts (Figure 7), which is also consistent with deep melting in the asthenosphere [e.g., *DePaolo and Daley*, 2000]. Before considering further implications, however, we need to assess the uncertainties in the correction scheme, the scatter in the data, and the uncertainty from heterogeneity in mantle source.

4.1. Uncertainties in the Melting Model

4.1.1. Uncertainties in the correction scheme. [30] The LKP model requires an estimate of the primary FeO and Na_2O concentrations to obtain the depth of mantle melting in a particular melting column. Because few of the B&R basalts are primary, we extrapolated measured compositions to primary ones by adding olivine until compositions were in equilibrium with mantle olivine (Fo_{89}). We accomplished this in two ways: one by starting with FeO at 8% MgO ($Fe_{8.0}$) and one by starting with the most primitive FeO in a given basaltic suite (Fe_{prim}). The two methods should yield similar results, however, if compositions >8% MgO are related to those at 8% MgO only by olivine addition. On the other hand, early crustal contamination (AFC) or multiple parental magmas will perturb these systematics, and in these cases the pressure/depth results from the two methods will be different. To test the effects of these factors on the melting depth calculation, we compared the depths derived from $Fe_{8.0}$ and Fe_{prim}. For 28 out of the 40 groups of basalts the difference in estimated melting depths between the two methods is <5 km. Ten out of the 40 groups of basalts show 5–10 km differences, and only two groups (SW border Nevada and Markagunt) show 10–13 km differences in estimated melting depths. In general, the difference in using Fe_{prim} and $Fe_{8.0}$ for most of the basalt groups clearly does not affect the overall mantle melting profile across the B&R and suggests that most high-MgO basalts within a given suite have fairly simple fractional crystallization histories and similar parental magmas. Because the primitive values (Fe_{prim}) typically require less olivine addition to extrapolate to primary compositions, we prefer the melting depth results calculated from Fe_{prim}, and these are shown in Figure 7 as the thick arrows (thin line extensions to the arrows, however, include depths calculated from $Fe_{8.0}$ and the $Fe_{8.0}$ errors, as discussed below).

4.1.2. Uncertainties derived from scatter in the FeO_t data. [31] Our approach in estimating melting depths was based on a single primary Fe content for each basaltic suite. While this approach minimizes the variety of AFC or magma mixing processes that can affect any single result, it also minimizes the information that can be derived from a suite of lavas by averaging potentially interesting variations. Each data array forms a scattered trend about the inferred fractionation trend, and this scatter was quantified by calculating an error ($Fe_{8.0-err}$; Table 1), based on the formal uncertainty about the regression. We can assess the effect of this scatter by calculating maximum ($Fe_{8.0} + Fe_{8.0-err}$) and minimum ($Fe_{8.0} - Fe_{8.0-err}$) melting depths. As seen in Figure 7 (thin line extensions to the thick arrows), these uncertainties have little effect on the overall systematic variations in mantle melting depth across the B&R. These uncertainties can be viewed either as an error on our calculations (generally 10 km error on both Z_o and Z_f) or as real variations recorded by distinct parental magmas in each suite. For example, a cluster of higher-Fe lavas from a given volcanic center may reflect magmas with a larger proportion of deep melts in the mixture or deeper overall melting than recorded by the average $Fe_{8.0}$ in the suite. It may be that finer-scale variations are preserved within each magma suite, analogous to the local versus global trends observed in the MORB data set [*Langmuir et al.*, 1992]. Whatever the exact cause, the ranges reflected in Figure 7 provide the maximum melting range that can be inferred from each volcanic center.

4.1.3. Uncertainties derived from variations in f_{O2}. [32] Our melting calculations assume that all Fe is Fe^{2+} (calculated as total FeO); this is clearly a poor assumption as significant Fe^{3+} may be present in alkali basalts. There are few actual measuraements of Fe_2O_3/FeO in Basin and Range basalts. Basalts in Mono basin have around 20–30% Fe^{3+}/Fe_T, leading to f_{O2} of −0.5 to 1.0 log units above nickel-nickel oxide (NNO) [*Lange et al.*, 1993; *Lange and Carmichael*, 1996]. Basalts from the eastern part of the study region, in SW Utah, record similar Fe^{3+}/Fe_T of around 18–25% [*Nusbaum et al.*, 1995]. Even more extreme oxidation occurs in the absarokites from Kings River, recording up to 50% Fe^{3+}/Fe_T and +1 to +3 NNO [*Feldstein and Lange*, 1999]. These values are overall higher than alkali basalts from Hawaii, which record Fe^{3+}/Fe_T of 12–14% and f_{O2} of −1 to 0 NNO [*Dixon et al.*, 1997; *Carmichael*, 1991]. In general, alkali basalts may have higher f_{O2} than tholeiites because Fe^{3+} behaves like an incompatible element, increasing in the melt as the extent of melting decreases. Hawaiian arch basalts show geochemical systematics consistent with this behavior [*Dixon et al.*, 1997] and a mantle source with Fe^{3+}/Fe_T within the range estimated by *O'Neill et al.* [1993] of 1.5–4%. Aside from the partial melting effect, however, basalts formed above subduction zones may have higher intrinsic f_{O2} [*Carmichael*, 1991], and basalts in the WGB may be so affected by prior subduction [*Lange et al.*, 1993]. Thus, in the lack of more data, Fe^{3+}/Fe_T ratios in Basin and Range basalts should vary with the extent of melting (which is fairly constant across the region at ~8%) and the effects of prior subduction (which are greatest in the west).

[33] The effect of Fe^{3+} on the melting calculations is to reduce the effective amount of FeO in the primitive melts and so lower all the pressure estimates. The magnitude of the effect can be estimated as follows. We take average F (8%) and apply this to the upper range of mantle Fe^{3+}/Fe_T estimated by *O'Neill et al.* [1993] of 4%, using the batch melting equation and a D of 0.2 for Fe^{3+} [*Dixon et al.*, 1997]. We then reduce FeO in the primary melt compositions to account for the Fe_2O_3 calculated. Although both the melt and mantle source FeO are reduced, the effect on the melt is greater, generally >10% Fe^{3+}/Fe_T, as compared to 4% in the mantle source. Thus the pressures of melting required to produce the lower FeO compositions are lower, on the order of 0.8–0.9 GPa lower in both P_o and P_f, or 25–30 km in depth. If we use the actual measured Fe^{3+}/Fe_T of the SW Utah basalts (Diamond Valley) of 18%, then the calculated pressures of melting are lower by 1.1 GPa (~33 km). An impossible solution is obtained for the Mono Basin using the Fe^{3+}/Fe_T of 35% measured by *Lange et al.* [1993]; melting would have to occur at <0.5 GPa (shallower than the Moho) to create 5 wt % FeO basalts. This can be reconciled by incorporating water in the mantle beneath Mono; *Lange et al.* [1993] estimate as much as 2–3 wt % H_2O in the basaltic magma based on the lowering of liquidus temperatures to 1100°–1200°C. These conditions are roughly similar to those created experimentally by *Hirose and Kawamoto* [1995] to generate basalts with 5–7 wt % FeO (at 1100°C and 1 GPa and 1.5–7 wt % H_2O in melt). Thus melting may well occur near the Moho, wet and cool, for Mono basalts.

[34] To summarize, converting some Fe^{2+} to Fe^{3+} will lower the estimates of the pressure of melting by as much as 1 GPa (20–30 km depth). But because the extent of melting does not vary systematically across the study region, the resulting effect on Fe^{3+} will not change the shape of the calculated melting region (merely raise it). If anything, the effect of f_{O2} is likely greatest in the western part of the study region, where prior subduction may have increased f_{O2} and H_2O in the mantle. This may only lead to even lower pressures of melting for the WGB and so an even greater contrast in the depths and temperatures of melting across the B&R. Clearly, more Fe^{3+}/Fe_T measurements are needed to refine the melting model.

4.1.4. Uncertainties in the mantle source composition. [35] The mantle beneath the B&R is certainly heterogeneous (Figure 6), and so an additional uncertainty is the mantle source composition. For our calculation of melting depth we chose an average fertile lherzolite with 15% clinopyroxene in the mode. What if the average mantle is actually more fertile or more refractory? The B&R peridotites vary systematically (Figure 6): as the mantle becomes more fertile (higher cpx), Na_2O increases, and as the mantle becomes more refractory (lower cpx), Na_2O decreases, while FeO remains fairly constant. Thus these variations have little effect on P_o (constrained by FeO) but a bigger effect on P_f and F (constrained by Na_2O). For example, choosing the most fertile mantle (19% cpx, 0.35 Na_2O) decreases P_f by ~0.15–0.2 GPa or decreases the top of the melting column by 4.5–6 km. The extent of melting will also increase by a few percent for this scenario, since P_o - P_f increases. The Na enrichment effect is somewhat compensated by an increase in K_d due to an increase in cpx. If we instead choose a more refractory mantle, typical of the average of all peridotites in Figure 6, (9% cpx; 0.16% Na_2O), then P_f increases by 0.3–0.45 GPa, or 10–15 km depth. However, in this scenario, F becomes vanishingly small (<1–2%) as smaller and smaller degrees of melting are required to produce high Na basalts from a Na depleted mantle. This average peridotite composition may be overly weighted to refractory mantle harzburgites, because mantle xenoliths preferentially sample the uppermost mantle, which in many cases has already lost a basaltic melt and/or been metasomatized. Thus, although we consider the simple average of all recovered xenoliths unreasonable for the source mantle of B&R basalts, it does provide a lower limit on the pressures and depths of melting (e.g., as P_f approaches P_o and F approaches 0). Taken together, the observed variations in mantle fertility may lead to 5–15 km uncertainty on the depth estimates; more fertile mantle leads to shallower melting, and more refractory mantle leads to deeper melting. If evenly distributed in space, these perturbations will not affect the overall observations of our study: that melting deepens toward the central B&R and most likely occurs below the lithosphere.

[36] We have interpreted Fe and Na variations in basalts across the B&R as reflecting changes in melting depth. Could some of these variations be due to a geographic variation in the composition of the mantle source? Figure 8 shows peridotite xenolith compositions plotted along the same transect as the basaltic data. The only obvious geographic systematics observed are the high FeO and abundance of harzburgites in the central B&R. This happens to be where the highest FeO basalts have erupted (e.g., Lunar Crater, Fortification Hill), and so it is possible that these basalt compositions reflect a high-FeO mantle source instead of great melting depths, as we have inferred above. There are several reasons, however, why these high-Fe peridotites may not be indicative of the mantle source. These xenoliths are from two volcanic fields: Lunar Crater, Nevada, and Wikieup, Arizona [*McGuire and Mukasa*, 1997; *Wilshire et al.*, 1988; *Bergman*, 1982]. The Wikieup xenoliths, however, include plagioclase harzburgites with low Mg # values more typical of crustal gabbroic rocks (Mg # < 80) and harzburgites that are too depleted in Na_2O (0.04 wt % on average) to generate basalts with >2.5 wt % Na_2O (e.g., F is negative). The isotopic and trace element systematics of all the Wikieup peridotites suggest extensive modification by basaltic melt infiltration, with the plagioclase peridotites recording the highest degrees of metasomatism [*McGuire and Mukasa*, 1997]. Although the Lunar

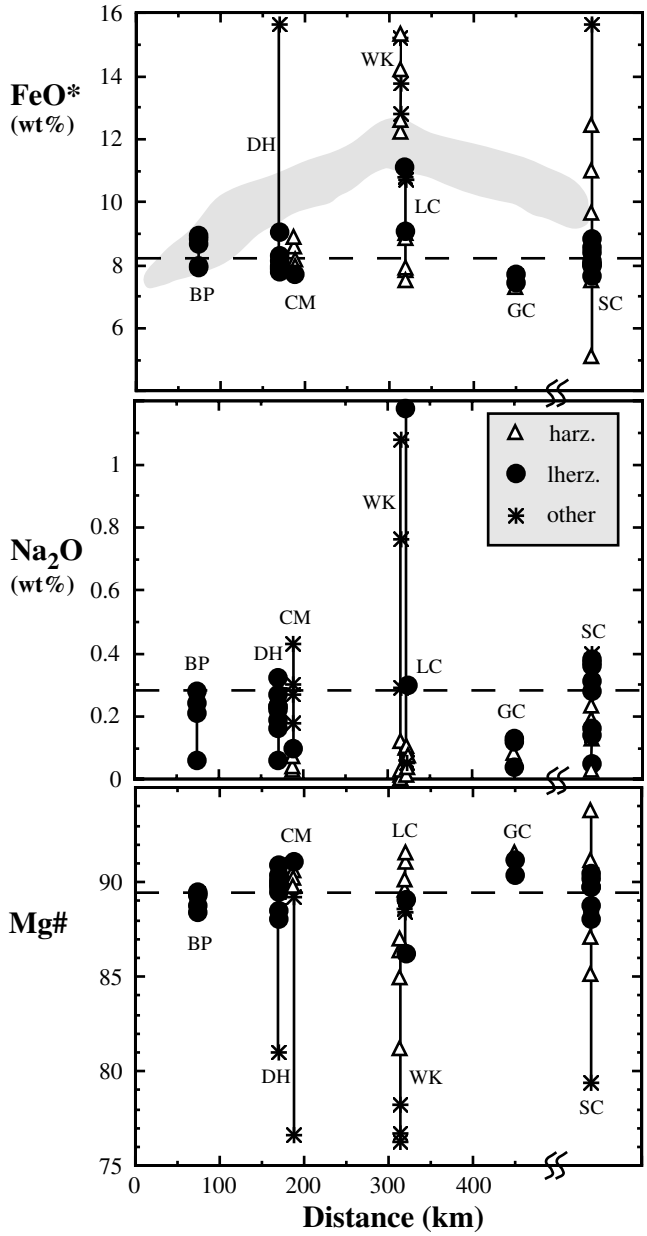

Figure 8. Peridotite xenolith whole-rock compositions across the Basin and Range and into the Colorado Plateau (distance along reference line from Figure 1). Lines connect samples from the same region: BP (Big Pine, California), DH (Dish Hill, California), CM (Cima, California), LC (Lunar Crater, Nevada), WK (Wikieup, Arizona), GC (Grand Canyon, Arizona), SC (San Carlos, Arizona). Data are from *Wilshire et al.* [1988]; *McGuire and Mukasa* [1997]; *Beard and Glazner* [1995]; *Smith et al.* [1999a]; *Frey and Prinz* [1978]; and *Bergman* [1982]. The dashed line is the average fertile lherzolite composition used to model mantle melting. "Other" peridotites include plagioclase peridotites, Al-augite peridotites, and dunites. The shaded field is basalt $Fe_{8.0}$ data (as in Figure 5; basalt $Na_{8.0}$ and Mg # are not plotted, as they are far outside of the peridotite range). San Carlos is on the opposite site of the Colorado Plateau, too far to project onto the distance line, but is included for reference.

Crater peridotites include some high-FeO compositions, the average FeO is 8.8 wt %, not significantly different than the value used in the melting model (8.2 wt %). Thus high Fe is not a general feature of these peridotites. Finally, if high-Fe (dense) mantle with Mg # of 85 were present in a large portion of the central B&R, it would be even more difficult to explain the high elevations and inferred high mantle buoyancy found there [e.g., *Humphreys and Dueker*, 1994b; *Jones et al.*, 1996]. Taken together, these high-Fe peridotites appear to be chemically disturbed and fall well outside the range of normal spinel lherzolites. Nonetheless, we can still consider the effect on the melting model for central B&R basalts if the mantle source consisted of an average of these peridotites (38.7 MgO, 12.5 FeO, 0.26 Na_2O, 14% cpx). The main effect of this high-Fe mantle source is to greatly decrease the pressure of melting (both P_o and P_f) while decreasing somewhat the degree of melting (due to the lower Na_2O). Depth of melting for central B&R basalts like Lunar Crater and Fortification Hill would decrease by 40–50 km. While these decreases are dramatic, they still predict melting significantly deeper (110–70 km) than melting in the WGB (70–40 km).

[37] A final kind of mantle heterogeneity involves the presence of garnet pyroxenite veins in the mantle [*Hirschmann and Stolper*, 1996]. In fact, *Beard and Johnson* [1997] have argued for garnet pyroxenites in the B&R source (for Cima, Lunar Crater, and West Mojave) to explain the combination of MORB-like Hf isotopes and steep REE patterns. Although mantle pyroxenites may explain some isotopic and trace element features of basalts, there are few pyroxenite melting experiments with which to predict the effect on major element compositions. *Hirschmann et al.* [1995] report high-FeO (11–13%) and low-SiO_2 (42–44%) melts derived from partial melting of garnet pyroxenites at 2.5 GPa, which is ~2.0 GPa lower pressure than that required to form the same high-FeO melts from peridotite. Thus pyroxenite melting may lead to lower pressures (and therefore temperatures) of melting than those calculated here. The FeO composition of pyroxenite melts, however, depends critically on the pyroxenite starting composition. Melting of MORB eclogites (more consistent with the scenario outlined by *Beard and Johnson* [1997]) leads to high-SiO_2 (>55%) and low-FeO (<9%) compositions (M. Pertermann and M. M. Hirschmann, manuscript in preparation) that are inconsistent with the high-FeO contents of the central and northern B&R lavas. Likewise, hydrous melts in equilibrium with garnet-cpx residues are uniformly high in SiO_2 (>52%) and Al_2O_3 (>17%) [*Rapp and Watson*, 1995], also unlike central and northern B&R lavas. Finally, pyroxenites are common in mantle xenoliths throughout the SW United States [e.g., *Wilshire et al.*, 1988], and it is unclear why their composition or abundance would vary systematically across the B&R to create the $Fe_{8.0}$ variation observed. Nonetheless, further melting experiments of pyroxenites and study of their abundance in mantle xenoliths are necessary to refine future melting inversions.

4.2. Summary of Major Element Results

[38] By inverting the FeO and Na_2O compositions of B&R basalts, we obtain a mantle melting profile across the B&R province. We emphasize that while the fractionation and melting schemes are similar conceptually to those developed for MORB, this is not a MORB model. In the fractionation correction we allow for natural variations in the liquid lines of descent for each suite of B&R basalts, and in the melting calculation we input mantle sources appropriate to the western United States. We also consider a simpler melting column, instead of the melting triangle typically modeled for MORB [*Plank and Langmuir*, 1992]. The results indicate shallowest melting (50–75 km) in the west and deepest melting (100–140 km) beneath the central and northern B&R, with a relatively smooth gradient in melting depth between these provinces (Figure 7). Farther east, toward the transition zone to the Colorado Plateau, melting shallows somewhat but generally remains >90 km. These variations are large relative to the uncertainties on the primary magma correction scheme (5–10 km), from the scatter in the Fe data (10–20 km), or from mantle fertility variations (5–15 km). Although high-Fe peridotites are found in the central B&R, these highly metasomatized compositions may reflect processes near the Moho more than compositions typical of the mantle melting regime. Thus the high-Fe basalts found in the central B&R are more likely due to deeper melting than to a high-Fe province in the mantle. Garnet pyroxenite melting could create some high-Fe compositions at lower pressures of melting, but this idea requires further melting and xenolith studies to evaluate. Errors involved in neglecting Fe^{3+} may raise the entire melting regime by as much as 20–30 km but will not change its shape across the B&R. In the following section we use REE data on basalts to provide an independent constraint on mantle melting parameters and test for consistency with the major element model.

4.3. Constraints From the Rare Earth Elements on Melting Depth

[39] Many studies have used the rare earth elements (REE) in basalts to constrain mantle melting depths regionally [e.g., *McKenzie and O'Nions*, 1991; *Ellam*, 1992; *Shen and Forsyth*, 1995; *Fram and Lesher*, 1997]. The utility of the REE in this regard derives mostly from their dramatic change in partitioning during melting of spinel peridotites versus garnet peridotites. This is due to garnet's strong preference for the heavy REE (HREE), and so melts in equilibrium with garnet have high Tb/Yb ratios. Because garnet is stable in mantle peridotite at higher pressures than spinel, the REE become a kind of geobarometer [e.g., *O'Neill*, 1981]. We have already noted that Tb/Yb in B&R basalts generally increases with $Fe_{8.0}$ (Figure 4), which is consistent with higher pressures of melting. The data do not show a one-to-one correlation between $Fe_{8.0}$ and Tb/Yb (Figure 9b), but this is to be expected since Tb/Yb will vary mostly in the garnet stability field, while $Fe_{8.0}$ will vary with pressure on either side of the spinel-garnet transition. The step to higher Tb/Yb (>1.8) at high $Fe_{8.0}$ (>10.5 wt %) is consistent with this prediction. Other studies based on trace element inverse modeling also find a variable role for garnet across the study area, from no residual garnet for low-FeO Big Pine basalts [*Ormerod et al.*, 1991] to garnet peridotite melting for some high-FeO basalts from the Colorado River Trough [*Bradshaw et al.*, 1993]. Here we test these ideas more quantitatively by using the pressures of melting calculated from Fe and Na contents to predict what the Tb/Yb of the B&R basalts should be. If the major element melting model is correct, then the predicted Tb/Yb should coincide with the observed Tb/Yb.

[40] In practice, modeling REE fractionation during mantle melting is complex. Realistic models would be polybaric along a melting adiabat, include changing modal mineralogy to reflect melting reactions, and use appropriate temperature-pressure- and composition-dependent partition coefficients (D). Unfortunately, appropriate partitioning data and peridotite melting reactions do not yet exist over the full range of melting pressures considered here (1.0–5.0 GPa). Thus our model is by necessity simple, yet it attempts to include the basic features of the melting column. As for the major element model, we model polybaric melting along an adiabat in a single mantle melting column, using P_o and P_f as calculated from Fe and Na, and a linear melt productivity term of 1.2% melting per kilobar of pressure decrease above the solidus. We approximate accumulated fractional melting by pooling batch melts at 1.2% increments. We start with a mantle mineral mode consistent with a fertile B&R lherzolite (Figure 6; actual values given in Figure 9) and use constant melting modes (assuming only cpx, garnet, and spinel enter the melt; the modes of olivine and orthopyroxene increase during melting, broadly consistent with possible melting reaction relationships [*Baker and Stolper*, 1994; *Salters and Longhi*, 1999]; values given in Figure 9). We assume a

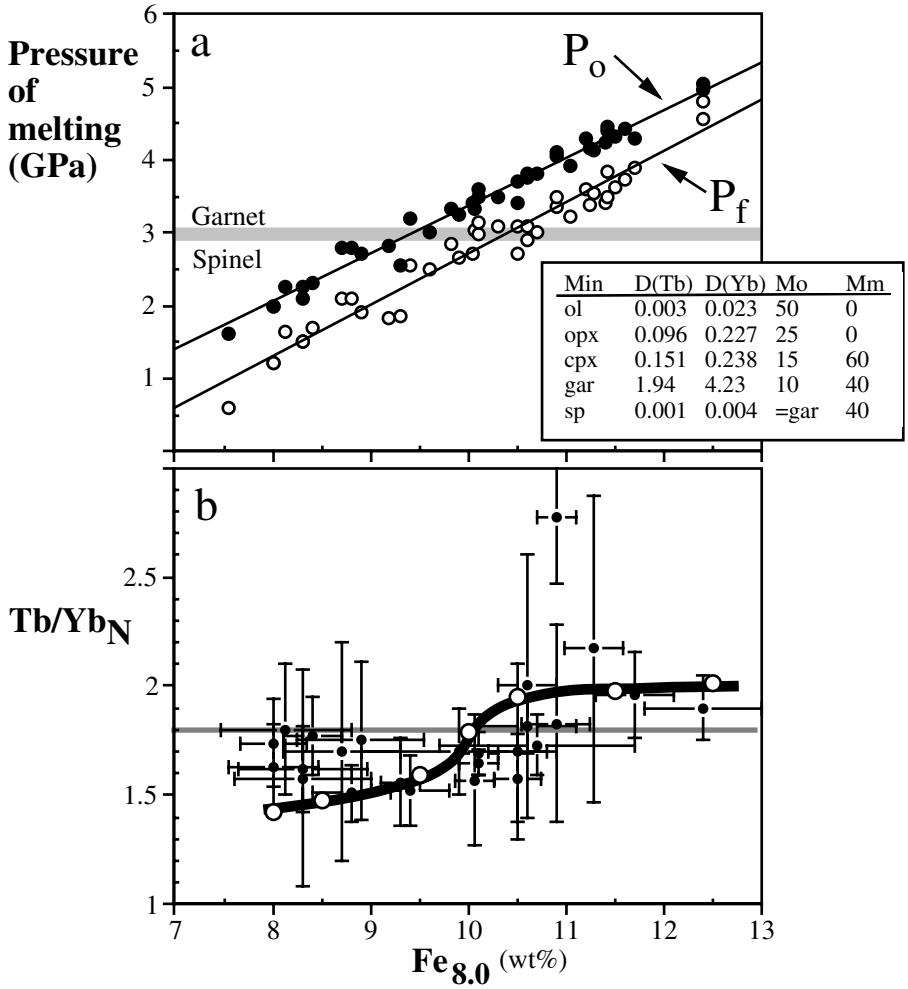

Figure 9. Relationship between $Fe_{8.0}$, Tb/Yb, and the pressure of melting in Basin and Range basalts (data and pressures in Table 1). (a) Lines are linear regressions of the pressure calculations, showing the average P_o (onset of melting) and P_f (final pressure of melting) for Basin and Range basalts. Shaded bar shows modeled garnet-spinel transition in peridotite at ~3.0 GPa. (b) Pressures of melting and gar-sp transition in Figure 9a are used to calculate the HREE fractionation (Tb/Yb) in mantle melts in Figure 9b. The model curve, shown as a heavy line through the open circles, is superimposed on basalt data (solid circles with error bars). The horizontal gray line shows that most basalts with Tb/Yb > 1.8 occur at $Fe_{8.0}$ > 10.5 wt %, where melting occurs entirely within the garnet peridotite stability field (from Figure 9a). All Tb/Yb are normalized to primitive mantle [*Sun and McDonough*, 1989]. Model parameters in box are for partition coefficients (D), initial mantle mode (M_o), and melting mode (M_m). Source composition is primitive mantle. Partition coefficients are from *Salters and Longhi* [1999] (for cpx, opx, and gar; at 2.8–3.0 GPa), and *Kelemen et al.* [1990] (for spinel and olivine).

primitive mantle starting composition for the REE [from *Sun and McDonough*, 1989], which is consistent with the average REE of SW United States peridotites [*Wang*, 1999].

[41] The critical partition coefficients for modeling REE during peridotite melting are for garnet, clinopyroxene, and orthopyroxene. We use the new high-pressure data (at 2.8–3.0 GPa) from *Salters and Longhi* [1999] for these three minerals (calculating D_{Tb} by interpolating between D_{Sm} and D_{Er}). Particularly noteworthy is the increasing "garnet-like" behavior of clinopyroxene at high pressure as it becomes richer in Ca-Tschermak [*Blundy et al.*, 1998] and Fe-Mg components [*Salters and Longhi*, 1999]. The other critical parameter is the pressure of the spinel to garnet transition. Recent studies place the transition on the solidus at 2.8–3.1 GPa, in both natural [*Robinson and Wood*, 1998] and simple systems (Ca-Mg-Al-Si [*Klemme and O'Neill*, 2000]). These transition pressures are also consistent with subsolidus results from *Koga et al.* [1999], based on an entirely different kinetic approach. We use 3.0 GPa as the transition pressure within our melting intervals and make the oversimplifying assumption that the transition occurs at a single pressure for all melting paths and that at the transition, garnet transforms to an equal quantity of spinel. Although neither of these assumptions is realistic, they do not have a large effect on the model. The actual transition from garnet to spinel may be narrow (0.1–0.2 GPa), and the slope of the transition above the solidus may be steep enough to have a comparably small effect on the transition pressure [*Robinson and Wood*, 1998]. The modal changes at the transition are clearly more complex than assumed, but the only important change to the bulk partitioning behavior is the disappearance of garnet.

[42] Results of the melting model are shown in Figure 9. To simplify the modeling, we observe that in the B&R basalts, $Fe_{8.0}$ scales linearly to both P_o and P_f (Figure 9a). The relationship between $Fe_{8.0}$ and P_o is expected; P_f also relates because F (at 7.9 ± 0.3% two sigma) and $Na_{8.0}$ (3.30 ± 0.05 wt %) are fairly constant across the region, and thus the interval $P_o - P_f$ is also fairly constant (at 0.65± 0.03 GPa). We use the linear relationships

shown in Figure 9a then to calculate HREE fractionation (Tb/Yb) as a function of $Fe_{8.0}$. The model curve broadly passes through the basalt data array (Figure 9b), adequately reproducing the lower Tb/Yb at low $Fe_{8.0}$ and the higher Tb/Yb at high $Fe_{8.0}$. Although the shape of the curve is not well constrained by the data, the model curve reproduces the step to higher Tb/Yb at $Fe_{8.0} > 10.5$ wt % owing to garnet dominance of the REE partitioning (line in Figure 9b). Melting columns above 10.5 wt % $Fe_{8.0}$ occur wholly in the garnet peridotite stability field ($P_f > 3.0$ GPa), while melting columns below 9.5 wt % $Fe_{8.0}$ occur wholly within the spinel peridotite stability field ($P_o < 3.0$ GPa). Thus the predictions of the major element model are consistent with the point at which the REE pattern of B&R basalts steepens (increasing Tb/Yb), and existing partition coefficients can broadly reproduce the range of HREE observed. While the model here is an over-simplification of the actual melting process, and the inclusion of some Fe^{3+} will lower *P* estimates, the HREE data confirm the pressures of melting calculated from the major element model as well as support the recent experimental work placing the spinel-garnet transition at >2.8 GPa.

5. Discussion

5.1. Comparison to Previous Geophysical/Geological Work

[43] In general, there is a good agreement between our calculated depths of melting and the position of the lithospheric lid, as inferred from some previous geophysical and geological studies. In Figure 7 our melting columns are superimposed on the mantle structure outlined by *Jones et al.* [1992], *Wernicke* [1992], and *Jones et al.* [1996]. Note that the tops of our melting columns coincide broadly with their asthenosphere-lithosphere boundary, consistent with the boundary serving as a rheological control on the upward limit of decompression melting. This boundary is based partly on geological arguments for a regional simple shear mechanism for extension, placing most of the lithospheric thinning beneath the Sierra Nevada region, while most of the crustal extension occurs to the east in the Central B&R. This view is generally supported by buoyancy calculations, which find a thinner lithospheric lid beneath the Sierra Nevada region and a thicker lithospheric lid beneath the Central B&R [*Jones et al.*, 1992, 1996; *Wernicke et al.*, 1996] (Figure 7). The great depths of melting we calculate for the few volcanic centers in the Northern B&R (Lunar Crater and Reveille Range), however, are inconsistent with the thin lithospheric lid calculated [*Jones et al.*, 1992, 1996]. Indeed, the revised estimates of *Jones et al.* [1996] yield negative lithospheric lid thicknesses, indicating extra mantle buoyancy in this area. The lid calculations put negative mantle buoyancy in the lithospheric lid thickness and do not include the possible effects of mantle temperature variations on buoyancy in the asthenosphere, which may be large (see below). Subsequent work by *Lowry et al.* [2000] estimates essentially no mantle lithosphere throughout the study area, but these calculations are based on a flexural model that attempts to propagate downward very thin elastic plate thicknesses (<15 km).

[44] Another relevant geophysical study [*Zandt et al.*, 1995] uses teleseismic *P* wave travel-time residuals recorded at 10 stations for a single event to constrain lithospheric lid thickness in a profile across the eastern part of our study area, from the Central B&R to the Colorado Plateau. These results place the lithosphere-asthenosphere boundary considerably shallower than the top of the melting region estimated here for the central Basin and Range. Even taking into account a maximum error of 35 km (corresponding to the maximum Fe^{3+} and Na source concentration), we would still calculate >100 km for the top of the melting region. *Zandt et al.* [1995] noted, however, that the seismic technique provides only relative residuals, with little constraint on the absolute depth to the lithosphere-asthenosphere boundary. Their shallower depths may be partly due to an a priori assumption that the average depth to the boundary is ~60 km. On the other hand, the depth step at the transition zone to the Colorado Plateau is probably a robust result of the seismic study, but this step in lithosphere thickness is also lacking in our results. We note few volcanic centers to constrain this transition, however, especially at the latitude (37°N) of the seismic study. Moreover, the main transition in lithosphere thickness modeled by *Lowry et al.* [2000, Plate 4] occurs well to the east of our data coverage. Finally, the step in *P* wave residuals could result from mantle temperature or composition differences instead of lithospheric lid thicknesses, as calculated by *Zandt et al.* [1995]. The difference in the relative residuals (0.2 s) could be explained quantitatively by a 100°C temperature difference between the B&R and Colorado Plateau asthenosphere, as predicted by our model (below; Figure 7), even without taking into account the slower P_n velocity (7.8 km/s versus 8 km/s) measured by *Lastowka et al.* [2001] for the B&R. The low-velocity zone found by *Lastowka et al.* [2001], however, is also shallower (55–65 km) than our predicted melting region (>100 km). This may mean that our melting region is not mapping the lithosphere-asthenosphere boundary or that the low-velocity zone derives from some other process than melting. Although our melting depths are more consistent with the mantle structure model presented by *Jones et al.* [1992, 1996], the *Zandt et al.* [1995] and *Lastowka et al.* [2001] models would still place most melting well below the lithosphere, in the asthenosphere.

5.2. Comparison to Previous Geochemical Work

[45] The depths of melting estimated by *Rogers et al.* [1995] are broadly consistent with those calculated here. On the basis of the SiO_2 content of near-primary basalts from Big Pine, *Rogers et al.* [1995] argued for melting depths of 45–75 km. We calculate 46–68 km on the basis of a completely different method using Fe and Na contents. In fact, the SiO_2 method is reasonably precise. Using the same *Hirose and Kushiro* [1993] data as *Rogers et al.* [1995], in addition to more recent peridotite melting data of *Baker and Stolper* [1994], *Robinson et al.* [1998], and *Walter* [1998], and limiting compositions to those of melt fraction 7–15% (most relevant to the B&R basalts), we obtain a good relationship between primary melt SiO_2 and melting pressure from 1 to 4 GPa (Figure 10a). If we calculate primary melt compositions by adding olivine to $Si_{8.0}$ and $Fe_{8.0}$ until the melt is in equilibrium with Fo_{89}, then we can obtain pressure estimates for each basaltic suite, simply from the SiO_2-*P* relationship shown in Figure 10a. While compositions <45% SiO_2 are not well calibrated, others produce average pressure estimates that agree reasonably well with the ranges calculated from Fe and Na (Figure 10b). This lends further support to the pressures calculated here, as the SiO_2 method is completely independent and involves minimal treatment of the data or assumptions.

[46] Other previous efforts to estimate mantle melting depths [e.g., *Perry et al.*, 1987; *Daley and DePaolo*, 1992; *DePaolo and Daley*, 2000] relied on normative compositions, namely, that alkali basalts (Ne normative) are derived from >50–60 km depth while tholeiites (Hy normative) are derived from <50–60 km depth. While this approach has formed the basis of several elegant papers that correlate isotopic variations to melting depths, there is much more information about the polybaric melting process that can be gleaned from a fuller suite of major and trace elements and recent experimental studies, as outlined here. Moreover, our new constraints on the depth of melting do not always agree with earlier inferences, based on "tholeiitic" versus "alkalic" designation. For example, our depths of melting calculated for the two tholeiitic basalts of *Daley and DePaolo* [1992] are considerably higher (120-95 km) than those based on the assumed depth range of tholeiite generation (<50–60 km). The SiO_2 method (Figure 10) also predicts greater depths of melting (70–90 km). The greater depths of melting are consistent with the high $Fe_{8.0}$ of these basalts,

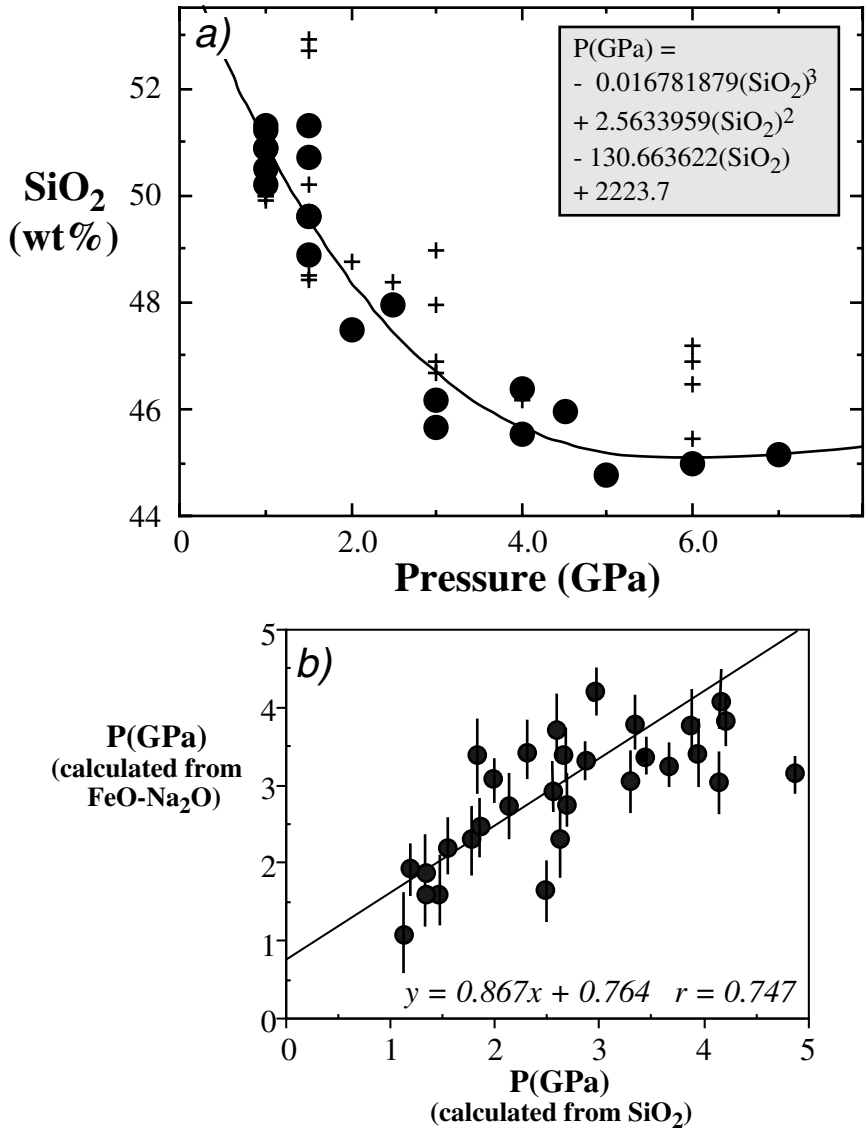

Figure 10. (a) Relationship between SiO_2 concentration of peridotite melts and melting pressure from laboratory experiments [*Hirose and Kushiro*, 1993; *Robinson et al.*, 1998; *Baker and Stolper*, 1994; *Walter*, 1998]. Plusses are all the experiments; large dots are for 7–15% melting only (appropriate to Basin and Range basalts). Equation given for empirical third-order polynomial fit. (b) Comparison of P of melting calculated from SiO_2 (based on Figure 10a) and from FeO-Na_2O (as in Figure 5) of Basin and Range basalts. Dots are for average P within the range from P_o to P_f (line). Line is fit only from 0 to 3.5 GPa (SiO_2 relationship is poorly constrained above 3.5 GPa, as shown in Figure 10a). Pressure offset may be due to an overestimation of P based on Fe (due to the assumption that all Fe is Fe2+) and/or an underestimation of P based on Si (due to the assumption of a single P of equilibration of polybaric melts).

although trace element data (Sc, full REE patterns) are lacking to test these ideas further.

[47] One reason for this discrepancy is that alkalinity and normative Ne are dependent on the total alkali ($Na_2O + K_2O$) as well as SiO_2 concentration. While SiO_2 does vary inversely with the pressure of peridotite melting (as demonstrated above), the alkalis depend on the degree of melting and the trace element heterogeneity in the source, neither of which may necessarily vary with the pressure of melting. In some situations the alkali effects may dominate. For example, reducing K_2O from 2.2 to 0.4 wt % and Na_2O from 3.5 to 2.7 wt % (still well within the range of B&R basalts) can create a quartz normative basalt from one that was Ne normative (based on sample 714-35 of *Daley and DePaolo* [1992]). Finally, although *DePaolo and Daley* [2000], (Figure 3) demonstrate that Ne has good sensitivity to melting pressures from 0.5 to 1.5 GPa, it discriminates poorly between pressures in the range relevant to subcontinental melting (1.5–3.0 GPa). On the other hand, SiO_2 and FeO vary greatly in this pressure range (Figures 5 and 10a) and so are better tools for estimating melting depth than Ne. Thus, although we agree in general that tholeiitic basalts may be derived from shallower depths than alkali basalts, this is a fairly blunt tool for assessing melting depths. A multielement approach, which takes advantage of newer experimental data, provides greater fidelity in modeling the melting process.

[48] Despite the differences in the inferred depths of melting between our work and that of *DePaolo and Daley* [2000], there are still some similarities in the conclusions. We both find evidence for thinned lithosphere and shallow melting beneath the eastern Sierras, with the lithosphere-asthenosphere boundary deepening to the east beneath Death Valley. The main difference in our results,

however, is the deep melting calculated here for the Lake Mead Extensional Area, contrasted with shallow melting and thinned lithosphere calculated by *DePaolo and Daley* [2000]. Their results, however, hinge on two tholeiitic samples erupted in the past 5 Myr with asthenospheric Nd isotopic composition. Following their interpretation, these lavas would require shallow melting of asthenosphere (<50 km) and therefore thinned lithosphere. We note, however, that these two tholeiites have SiO_2 and FeO very similar to the much more abundant Ne-normative basalts erupted at the same time (their Table 1), and so this compositional contrast derives more from variations in alkali content (as deduced from Rb) than a change in the elements that reflect variations in the depth of melting (SiO_2 and FeO). Even including these tholeiites, however, lavas erupted from the Lake Mead region over the past 7 Myr are predominantly alkalic and Ne-normative and have $\varepsilon_{Nd}>0$ (their Figure 11a), all consistent with deep, asthenospheric melting beneath a still thick lithosphere, as we have concluded.

[49] Most of the other previous geochemical work on B&R basalts has focused on isotopic and trace element ratios [e.g., *Kempton et al.*, 1991; *Ormerod et al.*, 1988; *Farmer et al.*, 1989; *Bradshaw et al.*, 1993; *Reid and Ramos*, 1996]. A basic paradigm of these studies is that basalts with enriched isotopic compositions (e.g., high $^{87}Sr/^{86}Sr$ and low $^{143}Nd/^{144}Nd$) and unusual trace element ratios (e.g., negative Nb anomalies) derive from the lithosphere, whereas basalts with oceanic island basalt (OIB)-like isotopic and trace element ratios derive from the asthenosphere. In this way, isotopes have been used indirectly to monitor the depth of melting and style of extension across the B&R. Whereas some of these isotopic variations are consistent with inferences based on tholeiitic and alkalic basalts (as discussed above) or $Si_{8.0}$ [*Rogers et al.*, 1995], much of this paradigm has been developed without accurate measures of the absolute depth of melting. There are also large uncertainties in trying to constrain lithospheric (shallow) versus asthenospheric (deep) melting on the basis of isotopic composition alone. For example, young lithosphere may not have a distinctive isotopic signature, and thermal conversion of lithosphere to asthenosphere may lead to "lithospheric" type isotopic compositions that derive from the asthenosphere (see discussion by *Beard and Johnson* [1997]). Our study represents a departure from most previous work in that it focuses specifically on those elements (Fe, Si, and REE) that can be used quantitatively to constrain the depth of melting.

[50] The major difference between our results and prior ones is that we infer melting to occur largely within the asthenosphere and that melting indeed stops at the base of the lithosphere owing to a rheological contrast, which halts mantle upwelling and melting. Our view is consistent not just with the lithospheric lid thicknesses discussed above but also with the modeling studies of *Harry and Leeman* [1995], which show difficulties in sustaining melting in the mantle lithosphere. The mantle lithosphere is generally too cold to melt, and so the only reasonable source of melts would be components with a lower solidus temperature than dry peridotite, such as mafic veins or hydrous components (e.g., amphibole or phlogopite peridotite). *Harry and Leeman* [1995] and *Harry et al.* [1993] argue that these components will produce melts during initial phases of extension and may be responsible for the widespread silicic volcanism during the Oligocene. However, during further extension, these lithospheric components are exhausted, and melting continues largely in the asthenosphere, generating the bimodal and predominantly basaltic volcanism during the past 10 Myr that we have modeled here.

[51] Thus, in accord with these models and with our results, we prefer the notion that melting across the B&R has occurred largely in the asthenosphere during the past 10 Myr. This is not to say that there has never been melting in the lithosphere. Prior to 10 Ma, silicic volcanism dominated over mafic, and enriched isotopic compositions dominated over depleted ones [e.g., *DePaolo and Daley*, 2000]; the melting regime may have been quite different. Indeed, in another paper (K. Wang et al., manuscript in preparation) we explore temporal variations that occur over a longer timescale (past 25 Myr) in the Colorado Trough-Lake Mead area and show evidence for a change in time from lithospheric to asthenospheric melting, similar to results from other studies of the SW United States [e.g., *Ormerod et al.*, 1988; *Daley and DePaolo*, 1992; *Feuerbach et al.*, 1993; *Bradshaw et al.*, 1993; *Faulds et al.*, 1999; *DePaolo and Daley*, 2000].

[52] The predominantly asthenospheric melting is in general agreement with Nd isotopic observations. The ruled bars in Figure 7 show those columns that generate melts with on average $\varepsilon_{Nd} > +0.5$, which may be more indicative of asthenospheric than old lithospheric sources. The high ε_{Nd} melting columns generally lie within the deeper parts of the melting profile, consistent with deeper asthenospheric melting. Most regions include mixed high and low ε_{Nd} basalts; thus there is a fair amount of evidence for either interaction within the overlying lithosphere or thermal conversion of old lithosphere to asthenosphere. The only region where average ε_{Nd} is uniformly less than +0.5 is in the western Great Basin, where melting is also shallowest. This might be taken as evidence for shallow melting in the lithosphere [e.g., *Rogers et al.*, 1995], but we argue (with others) below that much of the lithosphere is absent here and that melting also occurs in the asthenosphere.

5.3. Spatial Variations in the Depth of Melting Across the Basin and Range

[53] The essential features that emerge from our melting calculations are (1) the shallow depths of melting (50–75 km) in the western part of the region, beneath the eastern Sierra Nevada, and (2) the deep melting (>100 km) beneath the Central B&R-Colorado Plateau (Figure 7). Between these regions, melting depths follow a relatively smooth gradient. Below, we discuss the implications of these primary features of the melting profile.

5.3.1. Shallow melting beneath the Sierra Nevada region. [54] The shallowest melting occurs in the westernmost part of the melting profile, where some melting paths reach almost to the base of the crust. We interpret this to mean that mantle lithosphere is very thin in this area. Support for this view comes from the conceptual model of *Wernicke* [1992] and *Jones et al.* [1992], which places most of the mantle lithosphere thinning that accompanies B&R extension in the west, beneath the Sierra Nevada region. The excess buoyancy in this area combined with electrical conductivity, resistivity, and seismic measurements all support the interpretation that asthenosphere in the eastern Sierra Nevada and western margin of the Western Great Basin is shallow and mantle lithosphere is largely absent [*Wernicke et al.*, 1996; *Jones et al.*, 1996]. There are several models for the causes of thinning of the mantle lithosphere beneath the eastern Sierras. These fall into two general categories: (1) shear or foundering/delamination during Neogene extension [*Jones et al.*, 1992; *Ducea and Saleeby*, 1996] and (2) thermal erosion or delamination during Mesozoic/Cenozoic subduction [*Lee et al.*, 2000]. Better age constraints are needed to test whether one or both of these major tectonic episodes was the major cause of lithospheric thinning beneath the WGB/eastern Sierras.

[55] Independent support for recent thinning of the mantle lithosphere in this region comes from other thermobarometric and geochemical data. Xenoliths from the central Sierras (Big Creek) record Mesozoic replacement of lithosphere by asthenosphere, based on thermobarometry, Os isotopic compositions, and Ca zonation in orthopyroxenes [*Lee et al.*, 2000]. The timing of lithosphere replacement in the eastern Sierras is less clear, but mantle xenoliths from this region (some near the Big Pine volcanic field) record equilibration pressures that place them near the Moho (1.1–1.9 GPa) and record higher temperatures (1100°–1200°C) than those beneath the central Sierras (900°-750°C) [*Ducea and Saleeby*, 1996; *Lee et al.*, 2000]. Thus, the eastern Sierra xenoliths

are consistent with a recent influx of hot asthenosphere, perhaps during the Pliocene. The depths of melting we infer from basalts erupted in the eastern Sierras generally lie immediately beneath the depths recorded by the peridotites, which suggests that there may be a thin piece of mantle lithosphere above the melting regime that produces the basalts. Thus, taken together, the basalt and peridotite data provide support for recent (Mesozoic-Cenozoic) thinning of mantle lithosphere and shallow asthenospheric melting beneath the Sierras.

[56] Thin lithosphere and shallow melting are also consistent with normal mantle temperature in this region. The solidus temperature at 75 km is 1450°C [*Langmuir et al.*, 1992], requiring a mantle with potential temperature [*McKenzie and Bickle*, 1988] of ~1430°C. According to *McKenzie and Bickle* [1988], this is considerably hotter than "normal" mantle, which has a potential temperature (T_P) of 1280°C. Recent evidence, however, suggests that average T_p may be closer to 1400°–1425°C. *McKenzie and Bickle* [1988] derive T_p of 1280°C using high melt productivities (>1.5%/kbar) to generate oceanic crust of 7 km. Lower melt productivities [e.g., *Asimow et al.*, 1995] would require hotter mantle to generate the same thickness of ocean crust. *Stein and Stein* [1992] fit new oceanic heat flow and seafloor depth data with the GDH1 model that is consistent with T_p of 1420 at the base of the oceanic lithosphere, >100°C hotter than the *Parsons and Sclater* [1977] or *McKenzie and Bickle* [1988] model. *Anderson* [2000] uses a variety of evidence to suggest an average T_p in the upper mantle of 1400°C. On the basis of new experimental data, *Kinzler* [1997] calculates a solidus temperature of 1420°C at 2.0 GPa for average MORB, or T_p of ~1400°C. This is similar to our estimate of 1435°C at 2.2 GPa for primitive basalts near the Tamayo Fracture Zone, East Pacific Rise [*Bender et al.*, 1984], using the same algorithms as for the B&R calculations (Figure 7). Thus mantle temperature beneath the Western Great Basin is consistent with the nearby East Pacific Rise mantle and consistent with recent estimates of average upper mantle T_p of 1400°–1425°C.

[57] The presence of water in some WGB basalts [e.g., *Lange et al.*, 1993] may permit deeper melting than the dry solidus and thus deeper than calculated here. This may explain some of the high Tb/Yb values found in the WGB, although the general agreement between melting pressures calculated from FeO and SiO_2 argues for a fairly minor water effect. Moreover, *Feldstein and Lange* [1999] also estimate shallow melting depths (1.2–1.6 GPa) for Kings River magmas in the far western part of our profile, using an entirely different approach (Ba partitioning in phlogopite). This is in general agreement with the shallow depths calculated here from Fe-Na (1.6-0.6) and Si (1.1 GPa) for the same magmas. The presence of water may also have little effect on our temperature estimates, since *Gaetani and Grove* [1998] find that water has little effect distinct from temperature on the olivine K_d values. Thus, despite the complicating effect of water, the melting intervals calculated here for the WGB are consistent with normal mantle T_p and thinned lithosphere.

[58] Despite the strong evidence for shallow asthenosphere melting in this region, the isotopic composition of basalts from the western part of the region (eastern Sierras to the Western Great Basin) is not uniformly depleted. In fact, most basalts have enriched compositions, generally extending to negative ε_{Nd} values (e.g., Big Pine, Pinto Peak, and Crater Flat; see Table 1), indicating melting of old mantle components. Trace element ratios also indicate a nonasthenospheric mantle, and the standard interpretation is that these basalts derive from shallow depths in the enriched mantle lithosphere [e.g., *Ormerod et al.*, 1991; *Rogers et al.*, 1995]. Nonetheless, the overwhelming geophysical and xenolith data argue for very little mantle lithosphere in this area at this time. Therefore we prefer the interpretation that shallow melting beneath the WGB occurs in asthenospheric mantle, which may include thermally converted lithosphere or embedded old lithospheric remnants. Alternatively, melts derived in the asthenosphere could be contaminated by trace-enriched components in the thin overlying mantle lithosphere, thus affecting isotopic and incompatible trace element compositions without significantly disturbing major element components. These views are consistent with Nd isotopic values found in peridotite xenoliths from the area, which range from enriched to depleted compositions [*Beard and Glazner*, 1995], and Re-Os model ages, which range from Proterozoic to Phanerozoic [*Lee et al.*, 2000].

5.3.2. Deep, hot melting beneath the Central Basin and Range. [59] The deep melting predicted for the middle and eastern parts of the melting profile (Figure 7) derives from the high $Fe_{8.0}$, high Tb/Yb, and low SiO_2 of the Central and Northern B&R basalts. As discussed above, the presence of high-Fe peridotites could provide another explanation for the high-$Fe_{8.0}$ basalts, but most of these peridotite compositions appear to be the result of melt reaction, and are far removed from normal mantle compositions. Moreover, HREE, Al_2O_3, and SiO_2 compositions independently support deep (>100 km) melting in this region. Another alternative to generating high-Fe basalts involves melting of mantle garnet pyroxenites, but too little data exist at this time to evaluate this idea quantitatively.

[60] The final alternative to hot, deep melting is volatile melting. Adding CO_2 to peridotite can create some of the chemical characteristics seen in the central B&R basalts (e.g., low Al_2O_3 and SiO_2) but still requires deep (>3 GPa) and hot (>1500°C) melting [*Hirose*, 1997]. Previous subduction beneath western North America could have introduced H_2O into mantle, thus reducing the solidus temperature and enabling deep mantle melting along normal mantle adiabats. However, there are several problems with applying the wet melting model. First, volcanism in the Central B&R has gone on for the past 20 Myr despite the fact that the subducting slab retreated from the area >20 Myr ago [*Severinghaus and Atwater*, 1990]. It is difficult to see how wet melting can occur for such a period of time without replenishment of the water supply [*Harry and Leeman*, 1995]. Second, the isotopic and trace element compositions of the basalts that record melting >120 km (e.g. Lunar Crater, Lake Mead) are precisely those that have high ϵNd and trace element ratios (e.g., La/Nb) that are least like subduction-related lavas and most like OIB. Finally, hydrous peridotite melting produces low-FeO basalts [*Hirose and Kawamoto*, 1995; *Gaetani and Grove*, 1998] owing to the effect of lowering temperature on the olivine K_d values. Thus, in addition to the difficulty of producing high-FeO wet magmas, there is little evidence in these magmas for other subduction components to accompany the water. Several studies have concluded that these magmas look like OIB [e.g., *Fitton et al.*, 1991; *Kempton et al.*, 1991; *Lum et al.*, 1989; *Feuerbach et al.*, 1993], and so it is logical that they may require high melting temperatures as well.

[61] Thus the current evidence points toward hot, deep melting beneath the central B&R region. The mantle solidus at 135 km is ~1700°C [*Langmuir et al.*, 1992], requiring a potential temperature of ~1660°C. This is ~230°C hotter than the T_p of mantle melting beneath the western part of the study region, consistent with the temperature range calculated between normal MORB and hot spot basalts [*Klein and Langmuir*, 1987; *McKenzie and Bickle*, 1988; *Anderson*, 2000]. Thus melting beneath the central B&R requires mantle several hundreds of degrees hotter than normal asthenosphere. Although intersection of the East Pacific Rise with North America at ~20 Myr ago [*Atwater*, 1970] and slab window formation [*Glazner and Supplee*, 1982] provide mechanisms to bring asthenosphere to the region, normal East Pacific Rise asthenosphere is not hot enough to melt >70 km (Figure 7). The most obvious mechanism to introduce hot mantle is via a mantle plume. Although we find this mechanism somewhat ad hoc, there is abundant independent evidence in favor of active upwelling and/or hot mantle beneath central Nevada. Seismic imaging of *Humphreys and Dueker* [1994a, 1994b] indicates melting could be as deep as 200 km in the upper mantle of the B&R. This region possesses lower than average *S* velocities at a depth of 300 km [*van*

der Lee and Nolet, 1997], which might be expected for hot, deep mantle. *Savage and Sheehan* [2000] note an unusual pattern of shear-wave splitting in the Great Basin of Nevada, with a null region surrounded by a semicircular alignment of fast polarizations. They argue that this pattern, along with other supporting evidence (high dynamic elevation and high mantle buoyancy), is consistent with active mantle upwelling. Numerous studies have pointed out the excess mantle buoyancy in this region [*Jones et al.*, 1992, 1996; *Parsons et al.*, 1994; *Saltus and Thompson*, 1995; *Lowry et al.*, 2000], which is consistent with hotter-than-normal mantle. *Lowry et al.* [2000] suggest superadiabatic upwelling as one possible cause of dynamic elevation, but normal adiabatic ascent of hotter-than-normal mantle could also provide the excess buoyancy. Pyroxene compositions in peridotite xenoliths from Lunar Crater in central Nevada record equilibration temperatures 200°C higher than others from the western United States, which *Smith* [2000] interprets as evidence for a hot asthenosphere. Thus we disagree with *Bradshaw et al.* [1993] and conclude that the great melting depths calculated here for the B&R require something like a hot mantle plume.

[62] The closest large-scale hot spot to the central B&R is the Yellowstone hot spot, which has erupted basalts of the Snake River Plain. These basalts are remarkably similar in their major element composition to basalts of the central B&R [*Lum et al.*, 1989], with similar calculated depths and temperatures of melting (Figures 3 and 7). Thus one possibility is that the hot mantle beneath the central B&R is associated with the Yellowstone hot spot and that topography at the base of the lithosphere could drive its flow into the region [*Ebinger and Sleep*, 1998; *Humphreys et al.*, 2000]. Others [*Parsons et al.*, 1994; *Saltus and Thompson*, 1995] have argued that the excess mantle buoyancy in the region derives from the expansion of the Yellowstone plume head, which emerged 16–17 Myr ago. *DePaolo and Daley* [2000] show melting of asthenosphere with $\varepsilon_{Nd} \geq \sim 0$ at < 8–10 Ma for the Lake Mead, Death Valley, Colorado River, and Mohave areas, despite very different timing for extension in these regions. This could be consistent with the arrival of hot asthenosphere in the region at 8–10 Ma.

[63] Thus high mantle temperatures and a mantle plume are consistent with our results for deep melting beneath the central B&R. One apparent difficulty with this interpretation is that the volumes of magmatism in this region are quite small and not typical of voluminous plume melting. The volume of magmatism will be dependent, however, on the total length of the melting column, and not just mantle temperature. Thick lithosphere will restrict the upwelling path and lead to small volumes of magmatism, as observed. Thick lithosphere may also explain another potential inconsistency: the low heat flow in parts of Nevada [e.g., *Lowry et al.*, 2000]. Although the heat flow may be affected by crustal hydrology, the relatively recent arrival of the plume, coupled with a thick lithospheric lid, could also explain low heat flow in the area [*Saltus and Thompson*, 1995]. Another potential problem is that the region of deep melting identified here extends from central Nevada (Lunar Crater, Reveille Range) south to the Nevada-Arizona border (Lake Mead; western Grand Canyon), which has not been identified by other studies as a region of excess elevation, mantle buoyancy, or anomalous seismic structure. In fact, our deep melting region crosses the "elevation step" between the Northern and Central B&R [e.g., *Jones et al.*, 1992; *Saltus and Thompson*, 1995] and so would require different combinations of crustal thickness, lithosphere thickness, and mantle temperature to explain the topographic step and net mantle buoyancy change. Better resolution of these competing effects, and of the hot spot idea in general, could come from further seismic and heat flow studies extending from southern Nevada into Arizona as well as more chemical data on basaltic centers from this critical region (note ~15 centers without sufficient data in Figure 1).

[64] Finally, although the evidence for Yellowstone mantle beneath the B&R is suggestive, we note that other rifting regions show evidence for hot mantle upwelling that does not fit a classic hot spot/plume model. For example, *Kelemen and Holbrook* [1995] argue for higher than normal asthenospheric potential temperatures during rifting of the U.S. east coast margin. This thermal pulse did not occur near known hot spots, was not organized like a hot spot, and was relatively short-lived (5–8 Myr). Nonetheless, high seismic velocities and thicker than normal crust appear to require mantle potential temperatures several 100°C higher than normal during this phase of rifting. *King and Anderson* [1995] argue for small-scale convection at the edges of Archean lithosphere as an alternative cause of extension-related flood basalts. Continental insulation [*Anderson*, 1982; *Gurnis*, 1988; *Guillou and Jaupart*, 1995] is one mechanism to increase mantle temperature without calling on a deep-seated plume, but this generally requires a large, near-stationary continent far from the cooling effects of subduction, unlike the setting for the B&R. Long-term "incubation" (deep ponding without melting) of one or more plumes is another mechanism to create a thermal anomaly beneath thick continental lithosphere [e.g., *White and McKenzie*, 1989]. Thus the appearance of anomalously hot mantle is a common problem for many rifted margins and may relate to late Cenozoic B&R extension as well. Whether the upwelling beneath the thick lithosphere of the B&R is related to the Yellowstone plume or not may be tested with further seismic and petrologic data. The unique evidence contributed here from the Fe, Si, and Tb/Yb contents of B&R basalts, however, is that this upwelling mantle must be >200°C hotter than normal to generate melts from >120 km depth.

6. Conclusions

[65] 1. While crystal fractionation and crustal assimilation affect evolutionary trends in Basin and Range (B&R) magmatic suites, major element compositions at or above 8% MgO appear to reflect primary variations inherited from the melting process. Increasing $Fe_{8.0}$ and Tb/Yb, with decreasing $S_{i8.0}$ and $Al_{8.0}$, are consistent with deeper mantle melting from west to east across the B&R during the past 10 Myr.

[66] 2. The FeO and Na_2O contents of B&R basalts record polybaric decompression melting paths at 50–75 km beneath the Western Great Basin (WGB) and 100–140 km beneath the B&R, based on the melting model of *Langmuir et al.* [1992] and an average fertile B&R peridotite composition. The length of the melting column is fairly constant across the region, leading to 7.9 ± 0.3% melting on average (3.3–11.6% melting, full range). The HREE fractionation (Tb/Yb) in B&R basalts is consistent with the depths inferred from the major element melting model and for a spinel/garnet transition in peridotite around 3.0 GPa. These melting calculations provide more robust estimates of melting depth than previous work based on the isotopic compositions of "tholeiitic" and "alkali" basalts. SiO_2 is a better index than normative Ne of melting pressure.

[67] 3. The melting region beneath the B&R province during the past 10 Myr closely follows the lithosphere-asthenosphere boundary and places most melting paths in the asthenosphere, and not the lithosphere.

[68] 4. The shallow melting depths (50–75 km) beneath the WGB require substantially thinned mantle lithosphere, either due to thermal erosion during subduction in the Mesozoic or during extension in the Cenozoic. "Normal" mantle temperatures in this region are similar to those beneath the modern East Pacific Rise (T_p = 1430°C).

[69] 5. The high $Fe_{8.0}$ and Tb/Yb contents of basalts beneath the northern and central B&R leads to inferred deep melting (100–140 km). It is difficult to explain these compositions as the product of crustal contamination or volatile melting. Some mantle xenoliths from this region are unusually Fe-rich, and so it is possible that the high-Fe basalts result from high-Fe peridotites. These peridotites,

however, either are too depleted to yield alkali basalts or are the product of melt reaction. Moreover, a high-Fe mantle is inconsistent with the high mantle buoyancy in this region. Another possible mechanism for producing high-Fe basalts shallower in the mantle is the melting of certain kinds of garnet pyroxenite veins. This idea requires further study of xenoliths across the western United States and pyroxenite melting experiments to evaluate quantitatively. Thus, given the current evidence (including supporting evidence from high Tb/Yb and low SiO_2 compositions), we conclude that the high-Fe basalts from the northern and central B&R record deep peridotite melting which requires mantle potential temperatures >200°C above normal (T_p = 1660°C). These temperatures are consistent with a mantle plume or hot spot, for which other evidence exists in the form of excess mantle buoyancy, low seismic velocities, shear-wave splitting patterns, higher than normal peridotite mineral equilibration temperatures, and similarities in composition to the Snake River basalts associated with the Yellowstone plume.

[70] **Acknowledgments.** We thank Cin-Ty Lee, Marc Hirschmann, Geoff Abers, Craig Jones, Doug Smith, Lang Farmer, Tim Grove, Paul Wallace, and Drew Coleman for useful comments, unpublished data, and/or preprints. Formal reviews by Roberta Rudnick, Nick Rogers, and Doug Smith were both insightful and helpful. Plank acknowledges support from NSF OCE-9521717; Smith acknowledges support from the Nevada Nuclear Waste Project Office.

References

Alibert, C., A. Michard, and F. Albarede, Isotope and trace element geochemistry of Colorado Plateau volcanics, *Geochim. Cosmochim. Acta*, *50*, 2735–2750, 1986.

Anderson, D. L., Hotpsots, polar wander, Mesozoic convection and the geoid, *Nature*, *297*, 391–393, 1982.

Anderson, D. L., The thermal state of the upper mantle: No role for mantle plumes, *Geophys. Res. Lett.*, *27*, 3623–3626, 2000.

Asimow, P. D., M. M. Hirschmann, M. S. Ghiorso, M. J. O'Hara, and E. M. Stolper, The effect of pressure-induced solid-solid phase transitions on decompression melting of the mantle, *Geochim. Cosmochim. Acta*, *59*, 4489–4506, 1995.

Atwater, T., Implications of plate tectonics for the Cenozoic tectonics of western North America, *Geol. Soc. Am. Bull.*, *81*, 3513–3536, 1970.

Babcock, J. W., The late Cenozoic Coso Volcanic Field, Inyo County, California, Ph.D. thesis, Univ. of Calif., Santa Barbara, 1977.

Baker, M. B., and E. M. Stolper, Determining the composition of high-pressure mantle melts using diamond aggregates, *Geochim. Cosmochim. Acta*, *58*, 2811–2827, 1994.

Beard, B. L., and A. L. Glazner, Trace element and Sr and Nd isotopic composition of mantle xenoliths from the Big Pine volcanic field, California, *J. Geophys. Res.*, *100*, 4169–4179, 1995.

Beard, B. L., and C. M. Johnson, Hafnium isotope evidence for the origin of Cenozoic basaltic lavas from the southwestern United States, *J. Geophys. Res.*, *102*, 20,149–20,178, 1997.

Bender, J. F., C. H. Langmuir, and G. N. Hanson, Petrogenesis of basalt glasses from the Tamayo region, East Pacific Rise, *J. Petrol.*, *25*, 213–254, 1984.

Bergman, S. C., Petrogenetic aspects of the alkali basaltic lavas and included megacrysts and nodules from the Lunar Crater volcanic field, Nevada, USA, Ph.D. thesis, Princeton Univ., Princeton, N. J., 1982.

Best, M. G., and E. H. Christiansen, Limited extension during Peak Tertiary volcanism, Great Basin of Nevada and Utah, *J. Geophys. Res.*, *96*, 13,509–13,528, 1991.

Blaylock, J. P., E. I. Smith, and R. Holm, Geochemical investigation of Sunset Crater, Arizona: Complex petrogenetic history of a low-volume magmatic system, *Geol. Soc. Am. Abstr. Programs*, *28*, 162, 1996.

Blundy, J. D., J. A. C. Robinson, and B. J. Wood, Heavy REE are compatible in clinopyroxene on the spinel lherzolite solidus, *Earth Planet. Sci. Lett.*, *160*, 493–504, 1998.

Bradshaw, T. K., and E. I. Smith, Polygenetic Quaternary volcanism at Crater Flat, Nevada, *J. Volcanol. Geotherm. Res.*, *63*, 165–182, 1994.

Bradshaw, T. K., C. Hawkesworth, and K. Gallagher, Basaltic volcanism in the Southern Basin and Range: No role for a mantle plume, *Earth Planet. Sci. Lett.*, *116*, 45–62, 1993.

Carmichael, I. S. E., The redox state of basic and silicic magmas: A reflection of their source regions?, *Contrib. Mineral. Petrol.*, *106*, 129–141, 1991.

Cole, E. D., Petrogenesis of late Cenozoic alkalic basalt near the eastern boundary of the Basin-and-Range: Upper Grand Wash Trough, Arizona and Gold Butte, Nevada, M.S. thesis, Univ. of Nev., Las Vegas, 1989.

Coleman, D. S., and J. D. Walker, Geochemistry of Mio-Pliocene volcanic rocks from around Panamint Valley, Death Valley area, California, *Mem. Geol. Soc. Am.*, *176*, 391–411, 1990.

Cooper, J. L., and W. K. Hart, Mantle sources in the Arizona transition zone and global mantle heterogeneity, *Geology*, *18*, 1146–1149, 1990.

Daley, E. E., and D. J. DePaolo, Isotopic evidence for lithospheric thinning during extension: Southeastern Great Basin, *Geology*, *20*, 104–108, 1992.

Das, R., and G. Nolet, Crustal thickness map of the western United States, *J. Geophys. Res.*, *103*, 30,021–30,038, 1998.

DePaolo, D. J., and E. E. Daley, Neodymium isotopes in basalts of the southwest basin and range and lithospheric thinning during continental extension, *Chem. Geol.*, *169*, 157–185, 2000.

Dixon, J. E., D. A. Clague, P. Wallace, and R. Poreda, Volatiles in alkalic basalts from the North Arch volcanic field, Hawaii: Extensive degassing of deep submarine-erupted alkalic series lavas, *J. Petrol.*, *38*, 911–939, 1997.

Ducea, M., and J. Saleeby, Buoyancy sources for a large unrooted mountain range, the Sierra Nevada, California: Evidence from xenolith thermobarometry, *J. Geophys. Res.*, *101*, 8229–8244, 1996.

Dungan, M. A., M. M. Lindstrom, N. J. MacMillan, S. Moorbath, J. Hoefs, and L. A. Haskin, Open system magmatic evolution of the Taos Plateau volcanic field, northern New Mexico, 1, The petrology and geochemistry of the Servilleta basalt, *J. Geophys. Res.*, *91*, 5999–6028, 1986.

Ebinger, C. J., and N. H. Sleep, Cenozoic magmatism throughout east Africa resulting from impact of a single plume, *Nature*, *395*, 788–791, 1998.

Ellam, R. M., Lithospheric thickness as a control on basalt geochemistry, *Geology*, *20*, 153–156, 1992.

Embree, G. F., Lateral and vertical variations in a quaternary basalt flow: Petrography and chemistry of the Gunlock Flow, Southwestern Utah, *Brigham Young Univ. Geol. Stud.*, *17*, 67–117, 1970.

Farmer, G. L., F. V. Perry, S. Semken, B. Crowe, D. Curtis, and D. J. DePaolo, Isotopic evidence on the structure and origin of subcontinental lithospheric mantle in southern Nevada, *J. Geophys. Res.*, *94*, 7885–7898, 1989.

Farmer, G. L., A. F. Glazner, H. G. Wilshire, J. L. Wooden, W. J. Pickthorn, and M. Katz, Origin of late Cenozoic basalts at Cima volcanic field, Mojave Desert, California, *J. Geophys. Res.*, *100*, 8399–8415, 1995.

Faulds, J. E., E. I. Smith, and P. Gans, Spatial and temporal patterns of magmatism and extension in the Northern Colorado River Extensional Corridor, Nevada and Arizona: A preliminary report, in *Cenozoic Geology of the Northern Colorado River Extensional Corridor, Southern Nevada and Northwestern Arizona: Economic Implications of Regional Segmentation Structures*, edited by J. E. Faulds, pp. 171–183, Nev. Pet. Soc., Reno, Nevada, 1999.

Feldstein, S. N., and R. Lange, Pliocene potassic magmas from the Kings River region, Sierra Nevada, California: Evidence for melting of a subduction modified mantle, *J. Petrol.*, *40*, 1301–1320, 1999.

Feuerbach, D. L., Relationships between mid-Miocene volcanism and deformation of the lithosphere in the Northern Colorado River Extensional Corridor, Ph.D. thesis, 221 pp., Univ. of Iowa, Iowa City, 1998.

Feuerbach, D. L., E. I. Smith, J. D. Walker, and J. A. Tangeman, The role of the mantle during crustal extension: Constraints from geochemistry of volcanic rocks in the Lake Mead area, Nevada and Arizona, *Geol. Soc. Am. Bull.*, *105*, 1561–1575, 1993.

Fitton, J. G., D. James, P. D. Kepton, D. S. Ormerod, and W. P. Leeman, The role of lithospheric mantle in the generation of late Cenozoic basic magmas in the western United States, in *Oceanic and Continental Lithosphere: Similarities and Differences*, edited by M. A. Menzies and K. G. Cox, *J. Petrol.*, *29*, 331–349, 1988.

Fitton, J. G., D. James, and W. P. Leeman, Basic magmatism associated with late Cenozoic extension in the Western United States: Compositional variations in space and time, *J. Geophys. Res.*, *96*, 13,693–13,712, 1991.

Fram, M. S., and C. E. Lesher, Generation and polybaric differentiation of east Greenland early Tertiary flood basalts, *J. Petrol.*, *38*, 231–275, 1997.

Fraser, K. J., C. J. Hawkesworth, A. J. Erlank, R. H. Mitchell, and B. H. Scott-Smith, Sr-, Nd- and Pb-isotope and minor element geochemistry of lamproites and kimberlites, *Earth Planet. Sci. Lett.*, *76*, 57–70, 1985.

Frey, F. A., and M. Prinz, Ultramafic inclusions from San Carlos, Arizona: Petrologic and geochemical data bearing on their petrogenesis, *Earth Planet. Sci. Lett.*, *38*, 129–176, 1978.

Gaetani, G. A., and T. L. Grove, The influence of water on mantle melting, *Contrib. Mineral. Petrol.*, *131*, 323–346, 1998.

Gans, P. B., and W. A. Bohrson, Suppression of volcanism during rapid extension in the Basin and Range province, United States, *Science*, *279*, 66–68, 1998.

Glazner, A. F., and G. L. Farmer, Production of isotopic variability in

continental basalts by cryptic crustal contamination, *Science*, *255*, 72–74, 1992.

Glazner, A. F., and J. F. Supplee, Migration of Tertiary volcanism in the southwestern United States and subduction of the Mendocino fracture zone, *Earth Planet. Sci. Lett.*, *60*, 429–436, 1982.

Glazner, A. F., G. L. Farmer, W. T. Hughes, J. L. Wooden, and W. Pickthorn, Contamination of basaltic magma by mafic crust at Amboy and Pisgah Craters, Mojave Desert, California, *J. Geophys. Res.*, *96*, 13,673–13,691, 1991.

Guillou, L., and C. Jaupart, On the effect of continents on mantle convection, *J. Geophys. Res.*, *100*, 24,217–24,238, 1995.

Gurnis, M., Large-scale mantle convection and the aggregation and dispersal of super-continents, *Nature*, *332*, 695–699, 1988.

Harry, D. L., and W. P. Leeman, Partial melting of melt metasomatized subcontinental mantle and the magma source potential of the lower lithosphere, *J. Geophys. Res.*, *100*, 10,255–10,269, 1995.

Harry, D. L., D. S. Sawyer, and W. P. Leeman, The mechanics of continental extension in western North America: Implications for the magmatic structure of the Great Basin, *Earth Planet. Sci. Lett.*, *117*, 59–71, 1993.

Hauri, E. H., Major-element variability in the Hawaiian mantle plume, *Nature*, *382*, 415–419, 1996.

Hawkesworth, C. J., P. D. Kempton, N. W. Rogers, and P. W. van Calsteren, Continental mantle lithosphere, and shallow level enrichment processes in the Earth's mantle, *Earth Planet. Sci. Lett.*, *96*, 256–268, 1990.

Hawkesworth, C. J., S. Turner, K. Gallagher, A. Hunter, T. Bradshaw, and N. Rogers, Calc-alkaline magmatism, lithospheric thinning and extension in the Basin and Range, *J. Geophys. Res.*, *100*, 10,271–10,286, 1995.

Hirose, K., Partial melt compositions of carbonated peridotite at 3 GPa and role of CO2 in alkali-basalt magma generation, *Geophys. Res. Lett.*, *24*, 2837–2840, 1997.

Hirose, K., and T. Kawamoto, Hydrous partial melting of lherzolite at 1 GPa: The effect of H_2O on the genesis of basaltic magmas, *Earth Planet. Sci. Lett.*, *133*, 463–473, 1995.

Hirose, K., and I. Kushiro, Partial melting of dry peridotites at high pressures: Determination of compositions of melts segregated from peridotite using aggregates of diamond, *Earth Planet. Sci. Lett.*, *114*, 477–489, 1993.

Hirschmann, M. M., and E. M. Stolper, A possible role for garnet pyroxenite in the origin of the ''garnet signature'' in MORB, *Contrib. Mineral. Petrol.*, *124*, 185–208, 1996.

Hirschmann, M. M., M. B. Baker, and E. M. Stolper, Partial melting of mantle pyroxenite, *Eos Trans. AGU*, *76*(46), Fall Meet. Suppl., F696, 1995.

Hirschmann, M. M., M. S. Ghiorso, L. E. Wasylenki, P. D. Asimow, and E. M. Stolper, Calculation of peridotite partial melting from thermodynamic models of minerals and melts, I, Review of methods and comparison with experiments, *J. Petrol.*, *39*, 1091–1115, 1998.

Hirschmann, M. M., M. S. Ghiorso, and E. M. Stolper, Calculation of peridotite partial melting from thermodynamic models of minerals and melts, II, Isobaric variations in melts near the solidus and owing to variable source composition, *J. Petrol.*, *40*, 297–313, 1999.

Hoffine, S. R., Geochemistry of the volcanic rocks of the Saline Range, California: Implications for mantle composition and involvement in extension beneath the Basin and Range, M.S. thesis, Univ. of Kans., Lawrence, 1993.

Hofmann, A. W., Chemical differentiation of the Earth: The relationship between mantle, continental crust and oceanic crust, *Earth Planet. Sci. Lett.*, *90*, 297–314, 1988.

Humphreys, E. D., Post-Laramide removal of the Farallon Slab, Western United States, *Geology*, *23*, 987–990, 1995.

Humphreys, E. D., and K. G. Dueker, Western U. S. upper mantle structure, *J. Geophys. Res.*, *99*, 9615–9634, 1994a.

Humphreys, E. D., and K. G. Dueker, Physical state of the western U. S. upper mantle, *J. Geophys. Res.*, *99*, 9635–9650, 1994b.

Humphreys, E. D., K. G. Dueker, D. L. Schutt, and R. B. Smith, Beneath Yellowstone: Evaluating plume and nonplume models using teleseismic images of the upper mantle, *GSA Today*, *10*, 1–7, 2000.

Johnson, M. C., and T. Plank, 1999. Dehydration and melting experiments constrain the fate of subducted sediments, *Geochem. Geophys. Geosyst.*, vol. 1, Paper number 1999GC000014 [13,479 words, 10 figures, 8 tables]. December 16 2000.

Jones, C. H., Is extension in Death Valley accommodated by thinning of the mantle lithosphere beneath the Sierra Nevada, California?, *Tectonics*, *6*, 449–473, 1987.

Jones, C. H., and R. A. Phinney, Seismic structure of the lithosphere from teleseismic converted arrivals observed at small arrays in the southern Sierra, Nevada and vicinity, California, *J. Geophys. Res.*, *103*, 10,065–10,090, 1998.

Jones, C. H., B. P. Wernicke, G. L. Farmer, J. D. Walker, D. S. Coleman, L. W. McKenna, and F. V. Perry, Variations across and along a major continental rift: An interdisciplinary study of the Basin and Range Province, Western, USA, *Tectonophysics*, *213*, 57–96, 1992.

Jones, C. H., J. R. Unruh, and L. J. Sonder, The role of gravitational potential energy in active deformation in the southwestern United States, *Nature*, *381*, 37–41, 1996.

Kelemen, P. B., and W. S. Holbrook, Origin of thick, high-velocity crust along the U. S. east coast margin, *J. Geophys. Res.*, *100*, 10,077–10,094, 1995.

Kelemen, P. B., K. T. M. Johnson, R. J. Kinzler, and A. J. Irving, High-field-strength element depletion in arc basalts due to mantle-magma interaction, *Nature*, *345*, 521–524, 1990.

Kempton, P. B., M. A. Dungan, and D. P. Blanchard, Petrology and geochemistry of xenolith-bearing alkalic basalts from the Geronimo Volcanic Field, southeast Arizona: Evidence for polybaric fractionation and implications for mantle heterogeneity, in *Mantle Metasomatism and Alkaline Magmatism*, edited by E. M. Morris and J. D. Pasteris, *Spec. Pap. Geol. Soc. Am.*, *215*, 347–370, 1987.

Kempton, P. D., J. G. Fitton, C. J. Hawkesworth, and D. S. Ormerod, Isotopic and trace element constraints on the composition and evolution of the lithosphere beneath the southwestern United States, *J. Geophys. Res.*, *96*, 13,713–13,735, 1991.

King, S. D., and D. L. Anderson, An alternative mechanism of flood basalt formation, *Earth Planet. Sci. Lett.*, *136*, 269–279, 1995.

Kinzler, R. J., Melting of mantle peridotite at pressures approaching the spinel to garnet transition: Application to mid-ocean ridge basalt petrogenesis, *J. Geophys. Res.*, *102*, 853–874, 1997.

Kinzler, R. J., and T. L. Grove, Primary magmas of mid-ocean ridge basalts, 2, Application, *J. Geophys. Res.*, *97*, 6907–6926, 1992.

Klein, E. M., and C. H. Langmuir, Global correlations of ocean ridge basalt chemistry with axial depth and crustal thickness, *J. Geophys. Res.*, *92*, 8089–8115, 1987.

Klemme, S., and St. H. C. O'Neill, The near-solidus transition from garnet lherzolite to spinel lherzolite, *Contrib. Mineral. Petrol.*, *138*, 237–248, 2000.

Koga, K. T., N. Shimizu, and T. L. Grove, Disequilibrium trace element redistribution during garnet to spinel facies transformation, paper presented at 7th International Kimberlite Conference, Univ. of Cape Town, Rondebosch, South Africa, 1999.

Lange, R. A., and I. S. E. Carmichael, The Aurora volcanic field, California-Nevada: Oxygen fugacity constraints on the development of andesitic magma, *Contrib. Mineral. Petrol.*, *125*, 167–185, 1996.

Lange, R. A., I. S. E. Carmichael, and P. R. Renne, Potassic volcanism near Mono basin, California: Evidence for high water and oxygen fugacities inherited from subduction, *Geology*, *21*, 949–952, 1993.

Langmuir, C. H., E. M. Klein, and T. Plank, Petrological systematics of mid-ocean ridge basalts: Constraints on melt generation beneath ocean ridges, in *Mantle Flow and Melt Generation at Mid-Ocean Ridges*, *Geophys. Monogr. Ser.*, vol. 71, pp. 183–280, AGU, Washington, D. C., 1992.

Lastowka, L. A., A. F. Sheehan, and J. M. Schneider, Seismic evidence for partial lithospheric delamination model of Colorado Plateau uplift, *Geophys. Res. Lett.*, *28*, 1319–1322, 2001.

Leat, P. T., R. N. Thompson, M. A. Morrison, G. L. Hendry, and A. P. Dicjin, Compositionally-diverse Miocene-recent rift-related magmatism in northwest Colorado: Partial melting and mixing of mafic magmas from three different asthenospheric and lithospheric mantle sources, in *Oceanic and Continental Lithosphere: Similarities and Differences*, edited by M. A. Menzies and K. G. Cox, *J. Petrol.*, *29*, 351–377, 1988.

Lee, C.-T., Q.-Z. Yin, R. L. Rudnick, J. T. Chesley, and S. B. Jocobsen, Os isotopic evidence for Mesozoic removal of lithospheric mantle beneath the Sierra Nevada, California, *Science*, *289*, 1912–1916, 2000.

Livaccari, R. F., and F. V. Perry, Isotopic evidence for preservation of Cordilleran lithospheric mantle during the Sevier-Laramide orogeny, western United States, *Geology*, *21*, 719–722, 1993.

Lowry, A. R., N. M. Ribe, and R. B. Smith, Dynamic elevation of the Cordillera western United States, *J. Geophys. Res.*, *105*, 23,371–23,390, 2000.

Lum, C. C. L., W. P. Leeman, K. A. Foland, J. A. Kargel, and J. G. Fitton, Isotopic variation in continental basalt lavas as indicators of mantle heterogeneity: Examples from the western U.S. Cordillera, *J. Geophys. Res.*, *94*, 7871–7884, 1989.

McGuire, A. V., and S. B. Mukasa, Magmatic modification of the uppermost mantle beneath the Basin and Range to Colorado Plateau Transition Zone: Evidence from xenoliths, Wikieup, Arizona, *Contrib. Mineral Petrol.*, *128*, 52–65, 1997.

McKenzie, D., and M. J. Bickle, The volume and composition of melt generated by extension of lithosphere, *J. Petrol.*, *29*, 625–679, 1988.

McKenzie, D., and R. K. O'Nions, Partial melt distributions from inversion of rare earth element concentrations, *J. Petrol.*, *32*, 1021–1091, 1991.

Menzies, M. A., W. P. Leeman, and C. J. Hawkesworth, Isotope geochem-

istry of Cenozoic volcanic rocks reveals mantle heterogeneity beneath western USA, *Nature*, *303*, 205–209, 1983.
Menzies, M. A., P. Kempton, and M. Dungan, Interaction of continental lithosphere and asthenospheric melts below the Geronimo Volcanic Field, Arizona, USA, *J. Petrol.*, *26*, 663–693, 1985.
Nealey, L. D., J. R. Budahn, F. Maldonado, and D. M. Unruh, Geochemistry and petrogenesis of Quaternary basaltic rocks from the Red Hill and western Markagunt Plateau, southwestern Utah, in Geologic Studies in the Basin and Range-Colorado Plateau Transition in Southeastern Nevada, Southwestern Utah, and Northwestern Arizona, *U.S. Geol. Surv. Bull.*, *2135*, 179–184, 1997.
Niu, Y., and R. Batiza, An empirical method for calculating melt compositions produced beneath mid-ocean ridges for axis and off-axis (seamounts) melting application, *J. Geophys. Res.*, *96*, 21,753–21,777, 1991.
Nusbaum, R. L., D. M. Unruh, and V. E. Millings, The role of lithosphere and asthenosphere in the genesis of late Cenozoic volcanism at Diamond Valley and Veyo Volcano, southwestern Utah, in Geologic Studies in the Basin and Range-Colorado Plateau Transition in Southeastern Nevada, Southwestern Utah, and Northwestern Arizona, *U.S. Geol. Surv. Bull.*, *2135*, 229–239, 1995.
O'Neill, H. S. C., The transition between spinel lherzolite and garnet lherzolite, and its use as a geobarometer, *Contrib. Mineral. Petrol.*, *77*, 185–194, 1981.
O'Neill, H. S. C., D. C. Rubie, D. Canil, C. A. Geiger, C. R. Ross, II, F. Seifert, and A. B. Woodland, Ferric iron in the upper mantle and in transition zone assemblages: Implications for relative oxygen fugacities in the mantle, in *Evolution of the Earth and Planets, Geophys. Monogr. Ser.*, vol. 24, edited by E. Takahashi, pp. 73–88, AGU, Washington, D. C., 1993.
Ormerod, D. S., Late- to post-subduction magmatic transitions in the Western Great Basin, USA, Ph.D. thesis, 313 pp., Open Univ., Milton Keynes, England, U.K., 1988.
Ormerod, D. S., C. J. Hawkesworth, N. W. Rogers, W. P. Leeman, and M. A. Menzies, Tectonic and magmatic transitions in the Western Great Basin, USA, *Nature*, *333*, 349–353, 1988.
Ormerod, D. S., N. W. Rogers, and C. J. Hawkesworth, Melting in the lithospheric mantle: Inverse modeling of alkaline-olivine basalts from the Big Pine volcanic field, California, *Contrib. Mineral. Petrol.*, *108*, 305–317, 1991.
Parsons, B., and J. G. Sclater, An analysis of the variation of ocean floor bathymetery and heat flow with age, *J. Geophys. Res.*, *82*, 803–827, 1977.
Parsons, T., G. A. Thompson, and N. H. Sleep, Mantle plume influences on the Neogene uplift and extension of the U.S. western cordillera?, *Geology*, *22*, 83–86, 1994.
Perry, F. V., W. S. Baldrige, and D. J. DePaolo, Role of asthenosphere and lithosphere in the genesis of late Cenozoic basaltic rocks from the Rio Grande Rift and adjacent regions of the southwestern United States, *J. Geophys. Res.*, *92*, 9193–9213, 1987.
Plank, T., and C. H. Langmuir, An evaluation of the global variations in the major element chemistry of arc basalts, *Earth Planet. Sci. Lett.*, *90*, 349–370, 1988.
Plank, T., and C. H. Langmuir, Effect of the melting regime on the composition of the oceanic crust, *J. Geophys. Res.*, *97*, 19,749–19,770, 1992.
Rapp, R. P., and E. B. Watson, Dehydration melting of metabasalt at 8–32 kbar: Implications for continental growth and crust-mantle recycling, *J. Petrol.*, *36*, 891–931, 1995.
Reid, M. R., and F. C. Ramos, Chemical dynamics of enriched mantle in the southwestern United States: Thorium isotope evidence, *Earth Planet. Sci. Lett.*, *138*, 67–81, 1996.
Robinson, J. A., and B. J. Wood, The depth of the spinel to garnet transition at the peridotite solidus, *Earth Planet. Sci. Lett.*, *164*, 277–284, 1998.
Robinson, J. A. C., B. J. Wood, and J. D. Blundy, The beginning of melting of fertile and depleted peridotite at 1.5 GPa, *Earth Planet. Sci. Lett.*, *155*, 97–111, 1998.
Rogers, N. W., C. J. Hawkesworth, and D. S. Ormerod, Late Cenozoic basaltic magmatism in the Western Great Basin, *J. Geophys. Res.*, *100*, 10,287–10,301, 1995.
Salters, V. J. M., and J. Longhi, Trace element partitioning during the initial stages of melting beneath mid-ocean ridges, *Earth Planet. Sci. Lett.*, *166*, 15–30, 1999.
Saltus, R. W., and G. A. Thompson, Why is it downhill from Tonopah to Las Vegas?: A case for mantle plume support of the high northern Basin and Range, *Tectonics*, *14*, 1235–1244, 1995.
Savage, M. K., and A. F. Sheehan, Seismic anisotropy and mantle flow from the Great Basin to the Great Plains, western United States, *J. Geophys. Res.*, *105*, 13,725–13,734, 2000.
Scott, R. B., D. M. Unruh, L. W. Snee, A. E. Harding, D. L. Nealey, H. R. Blank Jr., and J. R. Budahn, Relation of Peralkaline magmatism to heterogeneous extension during the middle Miocene, southeastern Nevada, *J. Geophys. Res.*, *100*, 10,381–10,401, 1995.
Severinghaus, J., and T. Atwater, Cenozoic geometry and the thermal state of the subducting slab beneath western North America, in *Basin and Range Extensional Tectonics Near the Latitude of Las Vegas, Nevada*, edited by B. P. Wernicke, *Mem. Geol. Soc. Am.*, *176*, 1–22, 1990.
Shen, Y., and D. W. Forsyth, Geochemical constraints on initial and final depths of melting beneath mid-ocean ridges, *J. Geophys. Res.*, *100*, 2211–2237, 1995.
Smith, D., Insights into the evolution of the uppermost continental mantle from xenolith localities on and near the Colorado Plateau and regional comparisons, *J. Geophys. Res.*, *105*, 16,769–16,781, 2000.
Smith, D., J. C. A. Riter, and S. A. Mertzman, Water-rock interactions, orthopyroxene growth, and Si-enrichment in the mantle: Evidence in xenoliths from the Colorado Plateau, southwestern United States, *Earth Planet. Sci. Lett.*, *165*, 45–51, 1999a.
Smith, E. I., A. Sanchez, J. D. Walker, and K. Wang, Geochemistry of mafic magmas in the Hurricane volcanic field, Utah: Implications for small and large-scale chemical variability of the mantle, *J. Geol.*, *107*, 433–448, 1999b.
Stein, C. A., and S. Stein, A model for the global variation in oceanic depth and heat flow with lithosphere age, *Nature*, *359*, 123–129, 1992.
Sun, S. S., and W. F. McDonough, Chemical and isotopic systematics of oceanic basalts: Implications for mantle composition and processes, in *Magmatism in the Ocean Basins*, edited by A. D. Saunders and M. J. Norry, *Geol. Soc. Spec. Publ.*, *42*, 313–345, 1989.
Takahashi, E., and A. I. Kushiro, Melting of a dry peridotite at high-pressures and basalt magma genesis, *Am. Mineral.*, *68*, 859–879, 1983.
Till, R., Statistical Methods for the Earth Scientists-An Introduction, pp. 83–103, John Wiley, New York, 1974.
van der Lee, S., and G. Nolet, Upper mantle S velocity structure of North America, *J. Geophys. Res.*, *102*, 22,815–22,838, 1997.
Vaniman, D. T., B. M. Crowe, and E. S. Gladney, Petrology and geochemistry of Hawaiite lavas from Crater Flat, Nevada, *Contrib. Mineral. Petrol.*, *80*, 341–357, 1982.
Walker, J. D., and D. S. Coleman, Geochemical constraints on mode of extension in the Death Valley region, *Geology*, *19*, 971–974, 1991.
Walker, J. D., J. M. Fletcher, R. P. Fillmore, M. W. Martin, W. J. Taylor, A. F. Glazner, and J. M. Bartley, Connection between igneous activity and extension in the central Mojave metamorphic core complex, California, *J. Geophys. Res.*, *100*, 10,477–10,494, 1995.
Walter, M. J., Melting of garnet peridotite and the origin of komatiite and depleted lithosphere, *J. Petrol.*, *39*, 29–60, 1998.
Wang, K., Crustal-mantle interactions and mantle chemical systematics during Basin and Range extension, SW USA: Evidence from late Cenozoic volcanic rocks, Ph.D. thesis, 310 pp., Univ. of Kans., Lawrence, 1999.
Weaver, J. S., and C. H. Langmuir, Calculation of phase equilibrium in mineral-melt system, *Comput. Geosci.*, *16*, 1–19, 1990.
Wenrich, K. J., G. H. Billingsley, and B. A. Blackerby, Spatial migration and compositional changes of Miocene-Quaternary magmatism in the western Grand Canyon, *J. Geophys. Res.*, *100*, 10,417–10,440, 1995.
Wernicke, B., Cenozoic extensional tectonics of the U.S. Cordillera, in *The Geology of North America*, vol. G-3, *The Cordillera Orogen: Conterminous U.S.*, pp. 553–581, Geol. Soc. Am., Boulder, Colo., 1992.
Wernicke, B., G. J. Axen, and J. K. Snow, Basin and Range extensional tectonics at the latitude of Las Vegas, Nevada, *Geol. Soc. Am. Bull.*, *100*, 1738–1757, 1988.
Wernicke, B., et al., Origin of high mountains in the continents: the southern Sierra Nevada, *Science*, *271*, 190–193, 1996.
White, R., and D. McKenzie, Magmatism at rift zones: The generation of volcanic continental margins and flood basalts, *J. Geophys. Res.*, *94*, 7685–7729, 1989.
Wilshire, H. G., C. E. Meyer, J. K. Nakata, L. C. Calk, J. W. Shervais, J. E. Nielson, and E. C. Schawzman, Mafic and ultramafic xenoliths from volcanic rocks of the western United States, *U.S. Geol. Surv. Prof. Pap.*, *1443*, 1988.
Yogodzinski, G. M., T. R. Nauman, E. I. Smith, and T. K. Bradshaw, Evolution of a mafic volcanic field in the central Great Basin, south-central Nevada, *J. Geophys. Res.*, *101*, 17,425–17,445, 1996.
Zandt, G., S. C. Myers, and T. C. Wallace, Crust and mantle structure across the Basin and Range-Colorado Plateau boundary at 37°N latitude and implications for Cenozoic extensional mechanism, *J. Geophys. Res.*, *100*, 10,529–10,548, 1995.

T. Plank, Department of Earth Sciences, Boston University, 685 Commonwealth Avenue, Boston, MA 02215, USA. (tplank@bu.edu)
E. I. Smith, Department of Geosciences, University of Nevada, Las Vegas, Las Vegas, NV 89154, USA. (gsmith@ccmail.nevada.edu)
J. D. Walker and K. Wang, Department of Geology, University of Kansas, 120 Lindley Hall, Lawrence, KS 66045, USA. (jdwalker@ukans.edu; kefahuiwang@yahoo.com)